

served. These probes are not dephosphorylated by two protein tyrosine phosphatases (PTP1B and CD45) and serine/threonine phosphatases (PP1 and PP2A₁), but are slightly dephosphorylated by ALP. The widely used fluorescent phosphatase probe, DiFMUP, responds to all types of phosphatase activity; therefore, our new probes show different enzyme specificity from previously known probes. The enzyme kinetic data indicate that modification of the linker could dramatically change the enzyme affinity.

Our probe design strategy has afforded ACP-selective fluorescent probes. However, in principle, the probe structure can be changed significantly, provided that the hydroxy group (the 7-hydroxy group in this case) interacts with the ionic group (phosphate group in this case). Thus, this strategy should be applicable to the synthesis of fluorescent probes that are highly specific for various types of phosphatases by modifying the linker structure. Further, as discussed above, ratiometric fluorescent probes are preferable for quantitative bio-imaging experiments. As our probe design strategy intrinsically yields ratiometric probes, it should be helpful for the rational development of a wide range of fluorescent probes for the ratiometric bio-imaging of various hydrolases such as phosphodiesterases and sulfatase in living organisms.

Acknowledgements

This work was supported by MEXT of Japan (Grants 18310144 to K.K. and 19710185 to S.M.), the Special Coordination Funds for the Council of Science and Technology Policy (MEXT and JST), the Mitsubishi Foundation, the Shimadzu Science Foundation, the Kato Memorial Bioscience Foundation, the Astellas Foundation for Research on Metabolic Disorders, the Uehara Memorial Foundation, the Terumo Life Science Foundation, the Nagase Science and Technology Foundation, the Asahi Glass Foundation (to K.K.), and the Cosmetology Research Foundation (to S.M.). S.W. expresses his special thanks for The Global COE Program of Osaka University.

Keywords: coumarin · fluorescent probes · phosphatases · pK_a · ratiometric measurement

- [1] G. Gryniewicz, M. Poenie, R. Y. Tsien, *J. Biol. Chem.* **1985**, *260*, 3440–3450.
- [2] a) J. P. Y. Kao, A. T. Harootunian, R. Y. Tsien, *J. Biol. Chem.* **1989**, *264*, 8171–8178; b) H. Iatridou, E. Foukaraki, M. A. Kuhn, E. M. Marcus, R. P. Haugland, H. E. Katerinopoulos, *Cell Calcium* **1994**, *15*, 190–198.
- [3] R. Y. Tsien, T. J. Rink, M. Poenie, *Cell Calcium* **1985**, *6*, 145–157.
- [4] a) A. Miyawaki, J. Llopis, R. Heim, J. M. McCaffery, J. A. Adams, M. Ikura, R. Y. Tsien, *Nature* **1997**, *388*, 882–887; b) G. Zlokarnik, P. A. Negulescu, T. E. Knapp, L. Mere, N. Burres, L. Feng, M. Whitney, K. Roemer, R. Y. Tsien, *Science* **1998**, *279*, 84–88.
- [5] D. W. Moss, *Clin. Chem.* **1982**, *28*, 2007–2016.
- [6] D. W. Moss, F. D. Raymond, D. B. Wile, *Crit. Rev. Clin. Lab. Sci.* **1995**, *32*, 431–467.
- [7] S. Shenolikar, *Annu. Rev. Cell Biol.* **1994**, *10*, 55–86.
- [8] T. R. Burke, Z. Y. Zhang, *Biopolymers* **1998**, *47*, 225–241.
- [9] a) H. N. Fernley, P. G. Walker, *Biochem. J.* **1965**, *97*, 95–103; b) D. Robinson, P. Willcox, *Biochim. Biophys. Acta Enzymol.* **1969**, *191*, 183–186; c) J. M. Denu, D. L. Lohse, J. Vijayalakshmi, M. A. Saper, J. E. Dixon, *Proc. Natl. Acad. Sci. USA* **1996**, *93*, 2493–2498.
- [10] a) B. Rotman, J. A. Zderic, M. Edelstein, *Proc. Natl. Acad. Sci. USA* **1963**, *50*, 1–6; b) Z. Huang, Q. Wang, H. D. Ly, A. Govindarajan, J. Scheiget, R. Zamboni, S. Desmarais, C. Ramachandran, *J. Biomol. Screening* **1999**, *4*, 327–334.
- [11] S. Welte, K.-H. Baringhaus, W. Schmider, G. Müller, S. Petray, N. Tennagels, *Anal. Biochem.* **2005**, *338*, 32–38.
- [12] H. Takakusa, K. Kikuchi, Y. Urano, H. Kojima, T. Nagano, *Chem. Eur. J.* **2003**, *9*, 1479–1485.
- [13] K. R. Gee, W. C. Sun, R. H. Bhalgat, R. H. Upson, D. H. Klaubert, K. A. Latham, R. P. Haugland, *Anal. Biochem.* **1999**, *273*, 41–48.
- [14] Z. Huang, N. A. Olson, W. You, R. P. Haugland, *J. Immunol. Methods* **1992**, *149*, 261–266.
- [15] a) G. G. Guilbault, J. Hieserman, *Anal. Chem.* **1969**, *41*, 2006–2009; b) J. P. Goddard, J. L. Reymond, *Trends Biotechnol.* **2004**, *22*, 363–370.
- [16] D. W. Fink, W. R. Koehler, *Anal. Chem.* **1970**, *42*, 990–993.
- [17] W. C. Sun, K. R. Gee, R. P. Haugland, *Bioorg. Med. Chem. Lett.* **1998**, *8*, 3107–3110.
- [18] G. M. Huitink, D. P. Poe, H. Diehl, *Talanta* **1974**, *21*, 1221–1229.
- [19] M. Adamczyk, M. Cornwell, J. Huff, S. Rege, T. V. S. Rao, *Bioorg. Med. Chem. Lett.* **1997**, *7*, 1985–1988.

Received: April 7, 2009

Published online on May 22, 2009

Zinc is an essential trace element for spermatogenesis

Sonoko Yamaguchi^a, Chiemi Miura^a, Kazuya Kikuchi^b, Fritzie T. Celino^a, Tetsuro Agusa^{c,1}, Shinsuke Tanabe^c, and Takeshi Miura^{a,2}

^aResearch Group for Reproductive Physiology, South Ehime Fisheries Research Center, Ehime University, 1289-1, Funakoshi, Ainan, Ehime 798-4131, Japan; ^bGraduate School of Engineering, Osaka University, Osaka 565-0871, Japan; and ^cCenter for Marine Environmental Science, Ehime University, Matsuyama 790-8577, Japan

Edited by Ryuzo Yanagimachi, University of Hawaii, Honolulu, HI, and approved May 8, 2009 (received for review January 19, 2009)

Zinc (Zn) plays important roles in various biological activities but there is little available information regarding its functions in spermatogenesis. In our current study, we further examined the role of Zn during spermatogenesis in the Japanese eel (*Anguilla japonica*). Human CG (hCG) was injected into the animals to induce spermatogenesis, after which the concentration of Zn in the testis increased in tandem with the progression of spermatogenesis. Staining of testicular cells with a Zn-specific fluorescent probe revealed that Zn accumulates in germ cells, particularly in the mitochondria of spermatogonia and spermatozoa. Using an in vitro testicular organ culture system for the Japanese eel, production of a Zn deficiency by chelation with *N,N,N',N'*-tetrakis (2-pyridylmethyl)ethylenediamine (TPEN) caused apoptosis of the germ cells. However, this cell death was rescued by the addition of Zn to the cultures. Furthermore, an induced deficiency of Zn by TPEN chelation was found to inhibit the germ cell proliferation induced by 11-ketotestosterone (KT), a fish specific androgen, 17 α ,20 β -dihydroxy-4-pregnen-3-one (DHP), the initiator of meiosis in fish, and estradiol-17 β (E2), an inducer of spermatogonial stem-cell renewal. We also investigated the effects of Zn deficiency on sperm motility and observed that TPEN treatment of eel sperm suppressed the rate and duration of their motility but that co-treatment with Zn blocked the effects of TPEN. Our present results thus suggest that Zn is an essential trace element for the maintenance of germ cells, the progression spermatogenesis, and the regulation of sperm motility.

apoptosis | germ cells | in vitro culture | Japanese eel | sperm motility

Zinc (Zn) is well known as an essential trace element for a variety of biological activities. In biological systems, Zn is present in protein-bound and ionic forms, and plays important roles in mediating the function and structure of proteins, and in maintaining physiological balance. In vertebrates, Zn accumulates in the testis at high levels which are comparable to those in liver and kidney (1). In epidemiological studies in human, the inhibition of spermatogenesis and sperm abnormalities have been observed in patients with Crohn's disease and nutritional disorders, both of which induce a Zn deficiency (1–3). In vivo experiments in rodents have also demonstrated that a Zn deficiency can cause severe damage to the testes such as atrophy of the testicular tubules and the inhibition of spermatid differentiation (4, 5). Moreover, there are some reports that exposure to Zn can alleviate testis damage by stresses such as heavy metals, fluoride, and heat (6). These findings suggest that the testes may harbor a Zn-incorporation system, and that Zn itself may exert protective effect against testicular injury and play an essential role in the maintenance of testicular functions. However, there has been no evidence reported to date that shows any direct effects of Zn upon spermatogenesis in vertebrates.

In contrast to spermatogenesis, the effects of Zn on sperm motility have been examined in a number of vertebrate and invertebrate species. In humans, sperm motility declines in association with increased Zn concentrations in the seminal plasma (7). Morisawa and Yoshida have also reported that Zn in the seminal plasma of human suppresses sperm motility, and that

the removal of Zn by binding to a protein named semenogelin enhances motility (6). On the other hand, in sea urchin, treatment with the bivalent metal ion chelator, ethylenediamine tetra acetic acid (EDTA), inhibits sperm motility that is reversed by the addition of Zn (9). These results suggest that extracellular Zn indeed affects sperm motility but whether this is inhibitory or stimulatory appears to be species-specific. Additionally, it has been reported that Zn is present in sperm mitochondria and flagella (10, 11) but there had been no reports to date concerning the role of intracellular Zn upon sperm function.

To further study the role of Zn upon spermatogenesis in our current study, we chose Japanese eel (*Anguilla japonica*) as our animal model. In the Japanese eel in vivo, a complete pathway of spermatogenesis, from the spermatogonia stage to sperm maturation, can be induced by the injection of human CG (hCG; 12). Furthermore, we have developed a testicular organ culture system for the Japanese eel in our laboratory, which is the only currently available system of its kind in which the induction of complete spermatogenesis can be performed in vitro by the addition of 11-ketotestosterone or hCG (13, 14). By in vivo and in vitro analyses of spermatogenesis in the Japanese eel, we have previously further clarified the regulatory mechanisms underlying fish spermatogenesis (15, 16). Additionally, we have revealed the inhibitory effects of 4 trace elements (lead, molybdenum, rubidium, and arsenic) on fish spermatogenesis using our in vitro testicular organ culture system (17). In our present study, we again used the Japanese eel model to investigate the concentration and distribution of Zn in testis during spermatogenesis. Moreover we examined the effects of Zn addition and deficiency on spermatogenesis and sperm motility in vitro.

Results

Changes in the Levels and Distribution of Zinc (Zn) in the Testis of the Japanese Eel during Spermatogenesis. Before injection with hCG, the concentration of Zn in the testis of the Japanese eel was approximately 50 μ g/g. After injection, the Zn concentration in the testis gradually increased, and the highest levels were observed on day 9. Thereafter, the concentration of Zn remained at high levels until day 18 (Fig. 1).

To detect the distribution of Zn in eel testes, an unfixed testicular fragment was stained with a fluorescence sensor for Zn(II), ZnAF-2DA. Strong fluorescent signals were obtained in the lobules but not in the interstitial tissue (Fig. 2*A* and *B*). We thus further investigated the distribution of Zn in testicular tissue using isolated cells. Germ cells were found to be strongly stained

Author contributions: S.Y., C.M., and T.M. designed research; S.Y., C.M., F.T.C., T.A., S.T., and T.M. performed research; K.K. contributed new reagents/analytic tools; S.Y., C.M., and T.M. analyzed data; and S.Y., C.M., and T.M. wrote the paper.

The authors declare no conflict of interest.

This article is a PNAS Direct Submission.

¹Present address: Faculty of Medicine, Shimane University, Izumo, Shimane 693-8501, Japan.

²To whom correspondence should be addressed. E-mail: miutake@agr.ehime-u.ac.jp.

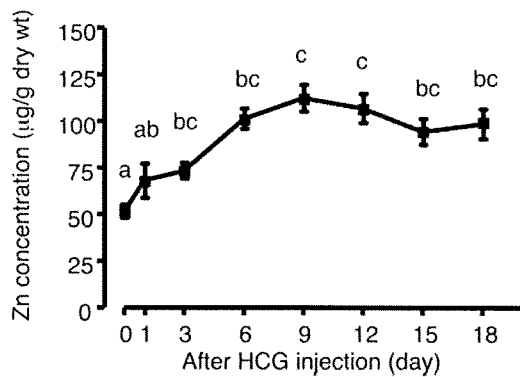


Fig. 1. Changes in the Zn concentrations in the testis of the Japanese eel after injection of human CG (hCG). The different letters indicate statistically significant differences ($P < 0.05$).

by ZnAF-2DA but Sertoli cells showed no signal (Fig. 2 C and D). When the germ cells were treated with 10 mM *N,N,N',N'*-tetrakis(2-pyridylmethyl) ethylenediamine (TPEN) for 1 h before staining with ZnAF-2DA, fluorescence was not detected (Fig. 2 E and F). We also stained the germ cells at various stages with ZnAF-2DA, that is, spermatogonia, spermatocytes, spermatids, and spermatozoa. ZnAF-2DA signals were detectable in spermatogonia, most notably in the mitochondria (Fig. 3 A–C). Additionally, the mitochondria of the spermatids and spermatozoa also displayed strong ZnAF-2DA signals (Fig. 3 D and E).

Effects of Zn and Zn Chelators on Japanese Eel Testes in Vitro. To investigate the putative key role of Zn during spermatogenesis, we analyzed the direct effects of Zn on the testis in the presence or absence of 11-ketotestosterone (KT). After culturing for 6 days, testicular fragments in the control group were found to be occupied by type A spermatogonia. Although the histological structure of the testicular fragments cultured with KT alone did not differ from the control group, the incorporation ratio of BrdU into the germ cells had significantly increased (Fig. 4), as

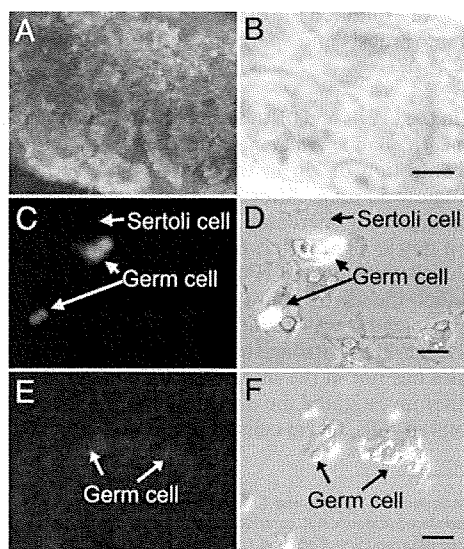


Fig. 2. The zinc distribution in the testis of the Japanese eel determined by staining with a Zn-specific fluorescent probe, ZnAF-2DA (A, C, and E). Bright field images are also shown (B, D, and F). (A and B) testicular fragments of the Japanese eel at 15 days after injection of hCG; (C and D) germ cells and Sertoli cells; (E and F) TPEN-treated germ cells. (Scale bars: A and B, 100 µm; C–F, 20 µm.)

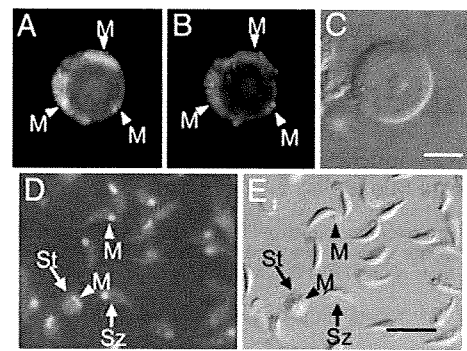


Fig. 3. Zinc distribution in germ cells of the Japanese eel. Zn was stained using ZnAF-2DA. Fluorescence images are shown for (A) Zn, and (B) mitochondria. (C) Bright field image of spermatogonia. (D) Zn fluorescence and (E) bright field image of spermatids and spermatozoa. M, mitochondria; St, spermatid; Sz, spermatozoa. (Scale bars: 10 µm.)

also reported in our previous study (13). Treatment of the Japanese eel testicular fragments with any level of Zn with or without KT did not affect the histology of the testis or the BrdU index (Fig. 4A). Treatment with ethylenediamine-*N,N,N',N'*-tetraacetic acid, calcium(II), disodium salt (Ca-EDTA), an extracellular Zn chelator, also did not affect the BrdU index or testicular morphology after 6 days in culture (Figs. 4B and 5B). In contrast, exposure to 0.01 and 0.1 mM TPEN, an intracellular chelator of Zn, inhibited BrdU-incorporation into germ cells (Fig. 4B), and induced germ cell death (Figs. 4B and 5C). Significantly, both the cell death and the inhibition of BrdU incorporation induced by TPEN was rescued by the addition of Zn (Figs. 4B and 5D). We further investigated the type of cell death that occurred using a TdT-mediated dUTP nick-end

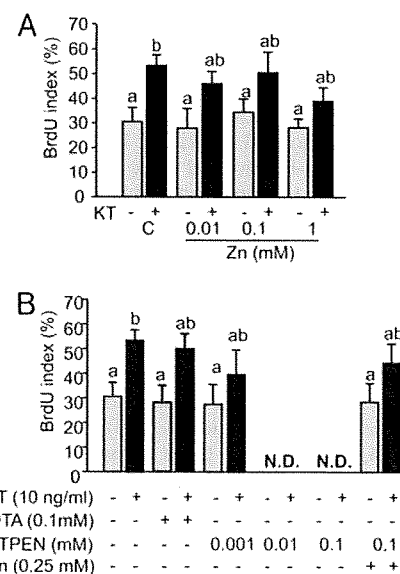


Fig. 4. Effects of Zn and Zn chelators on the early stages of spermatogenesis in vitro. The BrdU-labeling index was determined for germ cells in testicular fragments cultured with Zn (A) or Zn chelators (B) with or without KT. The number of BrdU-positive germ cells is expressed as a percentage of the total number of germ cells. C, control; Zn, ZnCl₂; KT, 11-ketotestosterone; TPEN, *N,N,N',N'*-tetrakis(2-pyridylmethyl)ethylenediamine; CaEDTA, ethylenediamine-*N,N,N',N'*-tetraacetic acid, calcium(II), disodium salt, dihydrate. Results are given as the mean ± SEM. The different letters on the columns indicate statistically significant differences ($P < 0.05$).

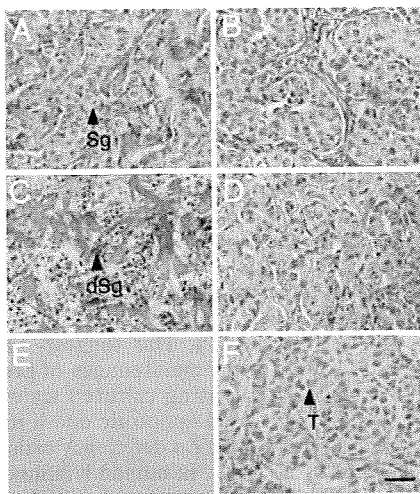


Fig. 5. Light micrographs of testicular fragments after culture with Zn chelators for 6 days. (A–D) Hematoxylin and eosin-stained testicular fragments cultured for 6 days. (A) control; (B) cultured with 0.1 mM CaEDTA; (C) cultured with 0.01 mM TPEN; (D) cultured with 0.1 mM TPEN and 0.25 mM ZnCl₂. (E and F) One-day cultures of testicular fragments subjected to a TUNEL assay. (E) control; (F) cultured with TPEN. Dark stained cells are TUNEL-positive (E and F). Sg, spermatogonia; dSg, dead spermatogonia; T, TUNEL-positive cells. (Scale bar: 20 μm.)

labeling (TUNEL) assay after a 1-day culture in the presence of TPEN. In the control and KT-treatment groups, no cell staining was observed (Fig. 5E). However, TUNEL-positive germ cells were detectable after treatment with 0.01–0.1 mM TPEN with or without KT (Fig. 5F).

We also investigated the effects of 0.001 mM TPEN, a dose that does not cause cell death, upon KT-induced spermatogenesis using our testicular organ culture system. Treatment with this dosage for 6 days had no effects on the histological structure of the testicular fragments. In contrast, after 15 days of this treatment, the testicular fragments were found to only have type A spermatogonia, although those cultured with KT alone contained the more progressed germ cells, type B spermatogonia (Fig. 6A–C). Importantly, the addition of Zn led to a recovery of spermatogenesis, such that the TPEN/KT treated cultures resembled those exposed to KT alone (Fig. 6D).

Effects of Zn on the Germ Cell Proliferation Induced by Various Steroid Hormones. In the Japanese eel, KT, 17 α ,20 β -dihydroxy-4-pregnen-3-one (DHP), and estradiol-17 β (E2) induce DNA

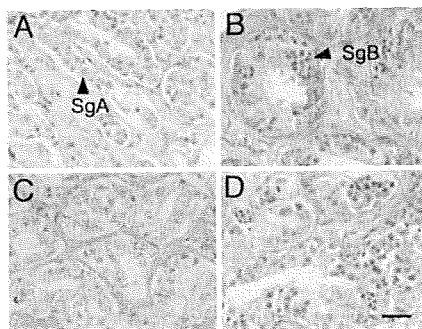


Fig. 6. Light micrographs of testicular fragments after culture with 10 ng/mL KT and 0.001 mM TPEN for 15 days. (A) Control; (B) cultured with 10 ng/mL KT; (C) cultured with KT and 0.001 mM TPEN; (D) cultured with KT, TPEN, and 0.0025 mM ZnCl₂. SgA, type A-spermatogonia; SgB, type B-spermatogonia. (Scale bar: 20 μm.)

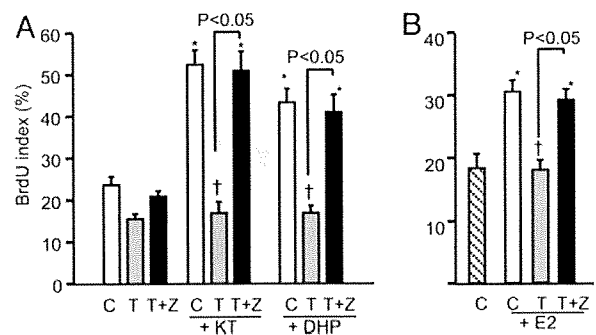


Fig. 7. Effects of a low dose TPEN upon germ cell proliferation in vitro. Testicular fragments were cultured with 0.001 mM TPEN and/or 10 ng/mL KT or DHP for 6 days (A) or cultured with TPEN and/or 1 ng/mL E2 (B). (C) Testicular fragments cultured without TPEN as a control for each steroid hormone; T, with TPEN; T+Z, with TPEN and Zn. KT, 10 ng/mL 11-ketotestosterone; DHP, 10 ng/mL 17 α ,20 β -dihydroxy-4-pregnen-3-one; E2, 1 ng/mL estradiol-17 β . Asterisks indicate significant differences from the negative control ($P < 0.05$). Daggers indicate significant differences from the control for each steroid hormone treatment ($P < 0.05$).

synthesis in germ cells thereby initiating spermatogenesis, meiosis, and spermatogonial stem-cell renewal, respectively (13, 16, 18). To elucidate at the stages of spermatogenesis at which Zn functions, that is, spermatogonial stem-cell renewal, spermatogonial proliferation or meiosis, we examined the effects of a 0.001 mM concentration of an intracellular Zn chelator on the germ cell proliferation induced by 10 ng/mL KT, 1 ng/mL E2, and 10 ng/mL DHP. These doses of KT, DHP and E2 were previously shown to be optimal for the induction of DNA synthesis in germ cells in vitro involving the initiation of spermatogenesis, meiosis, and spermatogonial stem-cell renewal, respectively (13, 16, 18). The rates of BrdU incorporation increased after treatment with KT and DHP for 6 days. However, treatment with 0.001 mM TPEN decreased the levels of BrdU incorporation induced by DHP or KT (Fig. 7A). To then investigate the effects of Zn on E2-induced germ cell proliferation, eel testes were cultured with E2 with or without 0.001 mM TPEN for 15 days according to the method of Miura et al. (18). Treatment with E2 alone significantly increased the number of BrdU-positive germ cells, whereas E2 in combination with 0.001 mM TPEN suppressed germ cell proliferation. This inhibition by TPEN was rescued by Zn treatment (Fig. 7B).

Effects of Zn Deficiency on Sperm Motility. In the mitochondria of Japanese eel sperm, strong ZnAF-2DA signals were observed. Hence, we analyzed the effects of Zn chelators on the rate and duration of eel sperm motility. Treatment of the sperm with Ca-EDTA did not alter their motility rate or duration at any concentration (Fig. 8A and B). In contrast, the addition of TPEN decreased both the motile rate and duration in a dose-dependent manner: 0.1–1 mM TPEN was found to be an effective concentration range for both indices. Furthermore, treatment with 1 mM Zn treatment rescued the inhibition of sperm motility by 1 mM TPEN (Fig. 8A and B).

Discussion

Some previous studies have reported that a high concentration of Zn is detectable in testis, and that a Zn deficiency inhibits spermatogenesis and causes sperm abnormalities (5, 19). However, there are currently few reports that address the function of Zn during spermatogenesis in any detail. We thus investigated in our current study the distribution of Zn in testis and the direct effects of Zn upon spermatogenesis using an in vitro testicular organ culture model derived from the Japanese eel.

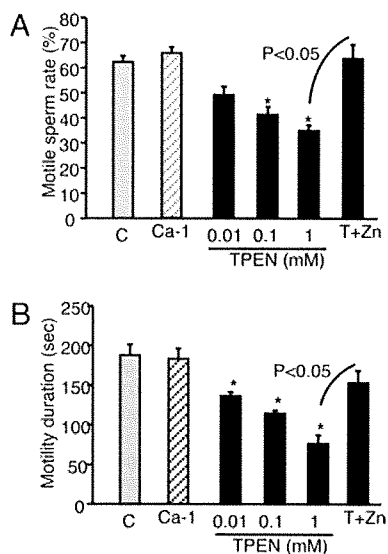


Fig. 8. Effects of Zn chelators on the motility of Japanese eel sperm. (A) Ratio of motile sperm; (B) duration of sperm motility. C, control; Ca-1, incubated with 1 mM Ca-EDTA; T+Z, incubated with 1 mM TPEN and 1 mM ZnCl₂. Asterisks indicate statistically significant differences from the control.

Our present analyses show that the Zn concentration in the testes of the Japanese eel gradually increases following an injection with hCG, and peaks on day 9 after this induction. Additionally, using a fluorescent Zn probe, strong signals were observed in germ cells, particularly spermatogonia, but not in the interstitial tissue or Sertoli cells. Similar to our present findings, Sørensen et al. have previously demonstrated by autometallography (AMG) that Zn is present in spermatogonia and primary spermatocytes in mouse (20). We previously demonstrated in our laboratory that a single injection of hCG first induced spermatogonial proliferation, then initiated meiosis on about day 12, and induced spermiogenesis on day 18 postinjection (12). Taken together therefore, our current data and previous findings suggest that Zn accumulates in the testis during early spermatogenesis, and may play a key role in the regulation of the spermatogonial proliferation and in the meiosis of germ cells. In the germ cells of other vertebrates, some Zn transporters have been observed. In rat, metallothionein (MT) was detected in spermatocytes (21) and other reports have shown that a testis-specific metallothionein-like protein (tesmin) is also present in these cells (22, 23). Additionally, Chi et al. have demonstrated that Zn accumulates in sperm in the mouse and that the Zn-exporter, ZnT-7, is present in the mouse testis, suggesting that Zn may be supplied to the germ cells via ZnT-7 (24). We speculate therefore that Zn may be accumulated in the germ cells of the Japanese eel via such transporter molecules.

In our present experiments in eel, Zn was found to accumulate prominently in the mitochondria in spermatogonia, spermatids and spermatozoa. In mouse, as detected via the AMG technique, sperm mitochondria were also previously shown to accumulate Zn, similar to our current results (10). Costello et al. have reported that Zn is imported into the mitochondria of prostate and liver cells in the form of a Zn-ligand complex such as Zn-citrate and Zn-MT (25, 26). Additionally, the membrane type Zn transporter protein ZnT-1 is expressed in the mitochondria of mouse spermatozoa (21). Taken together, there is now ample evidence to suggest that mitochondria may harbor a transporting system for Zn, and that Zn itself may have an important role to play in mitochondrial function in germ cells. In addition to

mitochondria, Zn has also been detected in other areas of the cytoplasm in eel spermatogonia. In rat, Zn accumulates in the cytoplasm of both spermatogonia and spermatocytes (20). Furthermore, murine ZnT-7 is present in Golgi apparatus of spermatocytes and spermatids (24). Thus, other organelles and cytosolic compartments may also accumulate Zn as part of its germ cell functions.

To further clarify the role of Zn in germ cells, we also investigated the effects of Zn and intra/extracellular Zn chelators on spermatogenesis using our *in vitro* testicular organ culture system developed from the Japanese eel. The results of these experiments demonstrated that treatment with the intracellular chelator TPEN caused germ cell death, which was blocked by the addition of Zn. This suggests that Zn is an essential trace element for the maintenance of germ cells. We performed a TUNEL assay using cultured testes and found that TPEN specifically caused apoptotic death in germ cells. There are some reports that a Zn deficiency causes apoptosis in various cell and tissue types. In human lymphocytes and rat hepatocytes for example, treatment with TPEN causes DNA fragmentation (27, 28). Interestingly, an *in vitro* and *in vivo* Zn deficiency was shown to induce caspase-3 activity in human mast cells and rat embryos, respectively (29, 30). Furthermore, treatment with Zn induces the antiapoptotic protein Bcl-2 and inhibits apoptosis in U947 cells (31). Caspase-3 and Bcl-2 in mitochondria have important roles in mitochondrial apoptosis; caspase-3 is released after cell damage and induces apoptosis, whilst Bcl-2 suppresses the apoptotic response (32). In our present study using a fluorescent Zn probe, we found that Zn accumulates in the mitochondria of germ cells and this may underpin its protection of these cells from apoptosis. However, the molecular mechanisms of how Zn regulates caspase-3 and Bcl-2 in mitochondria remain unclear at present. Some studies have addressed the correlation between Zn and apoptosis and suggest that Zn may function as an antioxidant in cells (32). Further studies will be necessary to clarify the role of Zn in the maintenance of germ cells.

We additionally investigated the influence of mild Zn deficiency on spermatogonial stem-cell renewal, spermatogonial proliferation, and meiosis *in vitro*. In a previous study, we reported that KT, E2, and DHP induce spermatogenesis, spermatogonial stem-cell renewal, and meiosis in eel germ cells, respectively (13, 15, 16). In our present report, TPEN was found to inhibit all steroid hormone-induced DNA synthesis in the testes of the Japanese eel. These results suggest that Zn has an important role in DNA synthesis involving mitotic cell proliferation and meiosis. A previous study using 3T3 cells has reported that treatment with the Zn chelator, diethylenetriaminepentaacetic acid, decreases the mRNA expression and activity of thymidine kinase, after which DNA synthesis was inhibited in 3T3 cells (33). Furthermore, steroid hormone receptors such as progesterin, androgen, and estrogen receptors all harbor Zn finger motifs within their structures (34). Other transcription factor genes containing Zn-finger motifs are also expressed during spermatogenesis (35). These findings suggest therefore that during steroid hormone-induced DNA synthesis, germ cells may incorporate Zn to activate a number of specific enzyme and Zn finger proteins, which are functionally disrupted by TPEN. Further analyses will be necessary to clarify the role of Zn on the functions of steroid hormone receptors and transcription factors during spermatogenesis.

Our current findings demonstrate that treatment with TPEN decreases sperm motility in the Japanese eel. Consistently in this regard, studies of human sperm have also demonstrated that diethyldithiocarbamate, which is an intracellular Zn chelator, inhibits sperm motility and decreases sperm velocity (36). These results suggest that intracellular Zn is important for sperm motility. As mentioned above, the mitochondria in the sperm of

the Japanese eel accumulate Zn. The ATP synthesized by the mitochondria is required for sperm flagella motility (37). Hence, Zn may have a function in mitochondrial ATP synthesis. Additionally, carbonic anhydrase (CA) is necessary for eel sperm motility, and this enzyme is expressed in the sperm membrane. CA catalyzes the reversible hydration of carbon and regulates the pH in various fluids. After spermiation, CA in the eel spermatozoa is activated after which it increases the pH and then induces sperm motility (15). CA is also known to be a Zn-binding protein, and its activity is dependent on the Zn concentration (38). Additionally, the removal of Zn from Zn-protein complexes extracted from human U87 human glioblastoma-astrocytoma cells by TPEN inhibited the function of the transcription factor, Sp1 (39). Although there is currently no information on effects of TPEN on CA activity, we speculate that TPEN may inhibit sperm motility by sequestering Zn away from this enzyme in sperm.

In conclusion, the results of our present study demonstrate that the Zn concentration in testis increases during spermatogenesis, and that Zn accumulates mainly in germ cells but not in either interstitial tissue or Sertoli cells. Our *in vitro* testicular organ culture experiments also demonstrated that a Zn deficiency causes the inhibition of DNA synthesis in germ cells, and induces an apoptotic response. Additionally, a Zn deficiency was found to suppress sperm motility in the Japanese eel animal model. These results suggest that Zn is an essential trace element for the maintenance and regulation of both spermatogenesis and sperm motility. However, the detailed mechanisms of Zn action during spermatogenesis remain to be clarified in further studies.

Materials and Methods

Animals. Cultivated male Japanese eels (180–200 g) were purchased from a commercial supplier and kept in a freshwater tank at 23 °C until use.

Measurement of Zn in Testis During Spermatogenesis. A previous report has indicated that hCG injection of a cultivated Japanese eel induces a complete cycle of spermatogenesis (11). Hence, these animals were injected with 1,000 IU/eel of hCG following anesthetization by ethylbenzoate. After injection, the fish were kept in a freshwater tank at 23 °C for 1, 3, 6, 9, 12, 15, and 18 days. Thereafter, hCG-injected eels ($n = 5$ for each day) were anesthetized and dissected, and the testes were collected and stored at –30 °C until measurement of Zn concentration. Before the experiments, testicular fragments were sampled from 5 uninjected eels as an initial control group. The testicular samples were dried for 12 h at 80 °C. For the analysis of Zn, dried testes were digested with HNO₃ in a microwave oven (ETHOS D, Milestone S.r.l.). The concentration of Zn was then measured using an inductively coupled plasma-mass spectrometer (ICP-MS; HP-4500, Hewlett-Packard).

Distribution of Zn in the Testis. We stained both the testicular fragments of the Japanese eel and the cells derived from these tissues with a Zn-specific probe. For this purpose, testis samples collected from the eels were cut into 100- μ m sections in ice-cold eel Ringer's solution using a Vibratome 3000 (Vibratome). Testicular cells were also prepared according to Miura et al. (40, 13, 16) for Zn staining. Briefly, testes were harvested and testicular cells were isolated by collagenase and dispase treatments. After treatment with DNase I, testicular cells were cultured in plastic culture dishes at 20 °C overnight and both fibroblasts and interstitial cells were allowed to adhere to the bottom of the dish, thus separating these cells from germ cells and Sertoli cells. The germ cells and Sertoli cells were then collected from the culture dishes and plated in collagen-coated dishes at 20 °C overnight. After this overnight culture, only the Sertoli cells adhere to the bottom of the dish. Thereafter, germ cells were collected in a test tube, and both the germ cells and Sertoli cell preparations were used to analyze the Zn distribution. Sertoli cells and germ cells could be identified using a variety of distinguishing characteristics and specific marker expression. Sertoli cells attached and spread to the bottom of the dish,

whereas germ cells did not attach and appeared spherical in shape. Furthermore, only germ cells express the progesterin receptor. We separated germ cells and Sertoli cells using this method previously (16).

Before staining of the germ cells, they were attached to a poly-L-lysine coated glass slide. Testicular fragments, attached germ cells and Sertoli cells were then washed 3 times in eel Ringer's solution, and incubated with 1 μ M of a permeable Zn-specific probe, Zn-AF 2DA (41) in eel Ringer's solution for 45 min at 20 °C. After this incubation, the cells were washed again in the Ringer's solution for 1 h at 20 °C and analyzed by fluorescence microscopy. The mitochondria of the spermatogonia were stained using MitoTracker Red (Invitrogen Co. Ltd.) according to the manufacturer's instructions with minor modifications before staining with Zn-AF 2DA.

In Vitro Testicular Organ Cultures. Organ cultures were prepared in accordance with the method of Miura et al. (13, 42). Male Japanese eels were dissected after anesthetization with ethylbenzoate. The testes were then collected, placed in ice-cold eel Ringer's solution and dissected into small pieces. Testicular fragments were placed on nitrocellulose membranes on top of cylindrical 1.5% agarose gels and set into a 24-well culture plate. Thereafter, 1 mL of Leibovitz' L-15 culture medium (Invitrogen Co. Ltd.) for eels (13) was added into each well with or without 0.01–1 mM ZnCl₂ (Zn), 0.001–0.1 mM TPEN, or 0.001–0.1 mM Ca-EDTA, which are intracellular and extracellular chelators of Zn, respectively, in combination with or without 10 ng/mL KT. The concentrations of Zn and chelators used in the *in vitro* experiments were based on the results obtained from the Zn measurement in the testis. Testicular fragments were incubated for 6 or 15 days and then fixed Bouin's solution for histological analysis.

Analysis of the Effects of a Mild Zn Deficiency upon Germ Cells. Testicular fragments were cultured with 0.001 mM TPEN in combination with 10 ng/mL KT, 1 ng/mL E2, and 10 ng/mL DHP for 6 or 15 days. Thereafter, testicular fragments were fixed and their histology was analyzed as described above.

Detection of Germ Cell Proliferation. The proliferation of Japanese eel germ cells was analyzed by immunohistochemical detection of 5-bromo-2-deoxyuridine (BrdU, Amersham Pharmacia Biotech) incorporation into replicating DNA. After culture for 6 or 15 days, testicular fragments were labeled with a 0.5 μ M BrdU solution for 18 h at 20 °C, and fixed in Bouin's solution. The fixed testicular fragments were then embedded in paraffin, cut into 4- μ m sections, and subjected to immunohistochemistry with a mouse monoclonal anti-BrdU antibody.

TdT-Mediated dUTP Nick-End Labeling (TUNEL) Assay. For the detection of apoptosis, the TUNEL assay was performed. One-day cultured testicular fragments were fixed in Bouin's solution, cut into 5 μ m-thick paraffin sections and then analyzed using an In Situ Cell Death Detection Kit (Roche Diagnostics, Ltd.) according to the manufacturer's instructions.

Effects of Zn on Sperm Motility. Eel sperm was collected after injection of the animals with hCG as described by Ohta et al. (43) and diluted 1:10,000 with artificial seminal plasma (149.3 mM NaCl, 15.2 mM KCl, 1.3 mM CaCl₂, 1.6 mM MgCl₂, and 10 mM NaHCO₃, adjusted to pH 8.2, see 43). The diluted sperm were then treated with 0.01–1 mM TPEN or 0.01–1 mM Ca-EDTA with or without 1 mM ZnCl₂ for 12 h at 4 °C. Thereafter, the sperm motility rate in seawater was measured as described previously (43). The duration of sperm motility was measured from 15 s after dilution in seawater until all movement had ceased completely.

Statistical Analysis. The results presented in this study are expressed as the mean \pm SEM. In instances where the data did not distribute normally, these values were converted to a logarithmic scale. Differences between the means were analyzed by 1-way analysis of variance followed by a Bonferroni multiple comparison test. Statistical analysis was performed using GraphPad Prism software (GraphPad Software inc.). In all cases, significance was set at $P < 0.05$.

ACKNOWLEDGMENTS. This study was supported by Grants-in-Aid for Scientific Research and for Fellows from the Japan Society for the Promotion of Science (JSPS), and by the Global COE Program from the Ministry of Education, Culture, Sports, Science and Technology (MEXT) of the Japanese government.

1. Bedwal RS, Bahuguna A (1994) Zinc, copper, and selenium in reproduction. *Cell Mol Life Sci* 50:624–640.
2. El-Tawil AM (2003) Zinc deficiency in men with Crohn's disease may contribute to poor sperm function and male infertility. *Andrologia* 35:337–341.

3. Prasad AS (2008) Zinc deficiency. *British Med J* 326:409–410.
4. Mason KE, Burns WA, Smith JC (1982) Testicular damage associated with zinc deficiency in pre- and postpubertal rats: Response to zinc repletion. *J Nut* 112:1019–1982.

5. Merker HJ, Günther T (1997) Testis damage induced by zinc deficiency in rat. *J Trace Element* 11:19–22.
6. Boran C, Ozkan KU (2004) The effect of zinc therapy on damaged testis in prepubertal rats. *Pediatr Surg Int* 20:444–448.
7. Henkel R, et al. (2005) Molecular aspects of declining sperm motility in older man. *Fert Ster* 84:1430–1437.
8. Morisawa M, Yoshida M (2005) Activation of motility and chemotaxis in the spermatozoa: From invertebrates to humans. *Reprod Med Biol* 4:101–114.
9. Clapper DL, Davis JM, Lamothe PJ, Patton C, Epel D (1985) Involvement of zinc in the regulation of pH_i, motility, and acrosome reactions in sea urchin sperm. *J Cell Biol* 100:1817–1824.
10. Stoltenberg M, et al. (1997) Autometallographic demonstration of zinc in rat sperm cell. *Mol Hum Reprod* 3:763–767.
11. Morisawa M, Mohri H (1972) Heavy metals and spermatozoan motility. I. distribution of iron, zinc and copper in sea urchin spermatozoa. *Exp Cell Res* 70:311–316.
12. Miura T, Yamauchi K, Nagahama Y, Takahashi H (1991) Induction of spermatogenesis in male Japanese eel, *Anguilla japonica*, by a single injection of human chorionic gonadotropin. *Zool Sci* 8:63–73.
13. Miura T, Yamauchi K, Takahashi H, Nagahama Y (1991) Hormonal induction of all stages of spermatogenesis *in vitro* in the male Japanese eel (*Anguilla japonica*). *Proc Natl Acad Sci USA* 88:5774–5778.
14. Miura T, Yamauchi K, Takahashi H, Nagahama Y (1991) Human chorionic gonadotropin induced all stages of spermatogenesis *in vitro* in the male Japanese eel (*Anguilla japonica*). *Dev Biol* 146:258–262.
15. Miura T, Miura C (2001) Japanese eel: A model for analysis of spermatogenesis. *Zool Sci* 18:1055–1063.
16. Miura T, Higuchi M, Ozaki Y, Ohta T, Miura C (2006) Progesterin is an essential factor for the initiation of the meiosis in spermatogenic cell of the eel. *Proc Natl Acad Sci USA* 103:7333–7338.
17. Yamaguchi S, et al. (2007) Effects of lead, molybdenum, rubidium, arsenic, and organochlorines on spermatogenesis in fish: Monitoring at Mekong Delta area and *in vitro* experiment. *Aquat Toxicol* 83:43–51.
18. Miura T, et al. (1999) Estradiol-17 β stimulated the renewal of spermatogonial stem cell in males. *Biochem Biophys Res Commun* 264:230–234.
19. Hidiroglou M, Knipfel JE (1984) Zinc in mammalian sperm: A review. *J Dairy Sci* 67:1147–1156.
20. Sørensen MB, et al. (1998) Histochemical tracing of zinc ions in the rat testis. *Mol Hum Reprod* 4:423–428.
21. Elgazar V, et al. (2005) Zinc-regulating proteins, ZnT-1, and Metallothionein I/II are present in different cell populations in the mouse testis. *J Histochem Cytochem* 53:905–912.
22. Sugihara T, Wadhwa R, Kaul SC, Mitsui YA (1999) novel testis-specific metallothionein-like protein, tesmin, is an early marker of male germ cell differentiation. *Genomics* 57:130–136.
23. Olesen C, Møller M, Byskov AG (2004) Tesmin transcription is regulated differently during male and female meiosis. *Mol Reprod Dev* 67:116–126.
24. Chi ZH, et al. (2009) ZNT7 and Zn²⁺ are present in different cell populations in the mouse testis. *Histol Histopathol* 24:25–30.
25. Guan Z, et al. (2003) Kinetic identification of a mitochondrial zinc uptake transport process in prostate cells. *J Inorg Biochem* 97:199–206.
26. Costello LC, Guan Z, Franklin RB, Feng P (2004) Metallothionein can function as a chaperone for zinc uptake transport into prostate and liver mitochondria. *J Inorg Biochem* 98:664–666.
27. Zelewski PD, Forbes IJ, Betts WH (1993) Correlation of apoptosis with change in intracellular labile Zn(II) using Zinquin [(2-methyl-8-p-toluenesulphonamido-6-quinolyloxy)acetic acid], a new specific fluorescent probe for Zn(II). *Biochem J* 296:403–408.
28. Nakatani T, Tawaramoto M, Kennedy DO, Kojima A, Matsui-Yuasa I (2000) Apoptosis induced by chelation of intracellular zinc is associated with depletion of cellular reduced glutathione levels in rat hepatocytes. *Chem-Biol Interact* 125:151–163.
29. Ho LH, et al. (2004) Labile zinc and zinc transporter ZnT4 in mast cell granules: Role in regulation of caspase activation and NF- κ B translocation. *J Immunol* 172:7750–7760.
30. Jankowski-Henning MA, Clegg MS, Daston GP, Rogers JM, Keen CL (2000) Zinc-deficient rat embryos have increased caspase 3-like activity and apoptosis. *Biochem Biophys Res Commun* 271:250–256.
31. Fukamachi Y, et al. (1998) Zinc suppresses apoptosis of U937 cells induced by hydrogen peroxide through an increase of the bcl-2/bax ratio. *Biochem Biophys Res Commun* 246:364–369.
32. Truong-Tran AQ, Carter J, Ruffin RE, Zelewski PD (2001) The role of zinc in caspase activation and apoptotic cell death. *Biometals* 14:315–330.
33. Chesters JK, Boyne R (1991) Nature of the Zn²⁺ requirement for DNA synthesis by 3T3 cells. *Experiment Cell Res* 192:631–634.
34. Freedman LP (1992) Anatomy of the steroid receptor zinc finger region. *Endocrine Rev* 13:129–145.
35. Rossi P, et al. (2004). Analysis of the gene expression profile of mouse male meiotic germ cells. *Gene Expr Patterns* 4:267–281.267–281.
36. Sørensen MB, Stoltenberg M, Danscher G, Ernst E (1999) Chelation of intracellular zinc ions affects human sperm cell motility. *Mol Human Reprod* 5:338–341.
37. Turner RM (2006) Moving to the beat: A review of mammalian sperm motility regulation. *Reprod Fert Develop* 18:25–38.
38. Supuran CT, Scozzafava A, Casini A (2003) Carbonic anhydrase inhibitors. *Med Res Rev* 23:146–189.
39. Rana U, et al. (2008) Zinc binding ligands and cellular zinc trafficking: Apo- metallothionein, glutathione, TPEN, proteomic zinc, and Zn-sp1. *J Inorg Biochem* 102:489–499.
40. Miura T, Ando A, Miura C, Yamauchi K (2002) Comparative studies between *in vivo* and *in vitro* spermatogenesis of Japanese eel (*Anguilla japonica*). *Zool Sci* 19:321–329.
41. Hirano T, Kikuchi K, Urano Y, Nagano T (2002) Improvement and biological applications of fluorescent probes for zinc, ZnAFs. *J Am Chem Soc* 124:6555–6562.
42. Miura C, Takahashi N, Michino F, Miura T (2005) The effects of *para*-nonylphenol on Japanese eel (*Anguilla japonica*) spermatogenesis. *In Vitro Aquat Toxicol* 71:133–141.
43. Ohta H, Izawa T (1996) Diluent for cool storage of the Japanese eel (*Anguilla japonica*) spermatozoa. *Aquaculture* 142:107–118.

Anion Sensor-Based Ratiometric Peptide Probe for Protein Kinase Activity

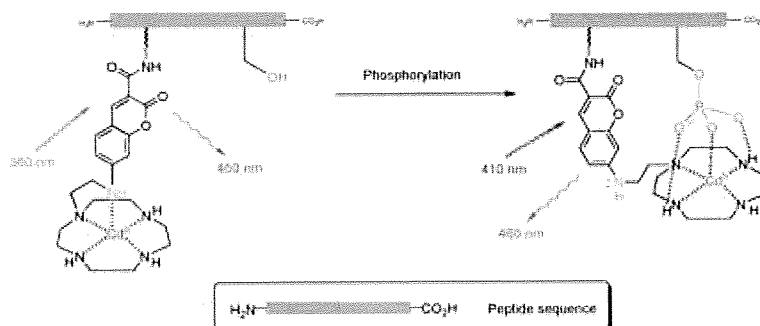
Kazuya Kikuchi,^{†,‡,§} Shigeki Hashimoto,^{†,‡} Shin Mizukami,^{‡,§} and Tetsuo Nagano^{*,‡}

Graduate School of Pharmaceutical Sciences, The University of Tokyo, 7-3-1 Hongo, Bunkyo-ku, Tokyo 113-0033, Japan and PRESTO, JST Corporation, Kawaguchi, Saitama, Japan

tlong@mol.f.u-tokyo.ac.jp

Received April 7, 2009

ABSTRACT



A new fluorescent sensor consisting of Cd^{II}-cylcen appended aminocoumarin and a substrate peptide for protein kinase A (PKA) has been designed. Upon phosphorylation by PKA, the metal complex moiety binds to a phosphorylated residue, which in turn displaces the coumarin fluorophore, and this event results in ratiometric change of excitation spectrum in neutral aqueous solution.

Signal transduction pathways provide mechanisms for transducing external signals to intracellular biological responses. Protein kinases modulate the activity of their target proteins by phosphorylating serine, threonine and tyrosine residues within the intact proteins in these pathways. A great number of kinases have been discovered, and the characterization of their roles in complicated signaling pathways is now a very active research area.¹ The development of an analytical tool that can enable monitoring of the temporal and spatial dynamics of cellular kinases would therefore contribute substantially to a better understanding of signal transduction mechanisms.²

Various approaches to monitor the activities of protein kinases have been made,^{3,4} one of which is the use of fluorophore-labeled peptide substrates.⁵ Traditional peptide probes contain a polarity-sensitive fluorophore near the site

(3) (a) Nagai, Y.; Miyazaki, M.; Aoki, R.; Zama, T.; Inouye, S.; Hirose, K.; Iino, M.; Hagiwara, M. *Nat. Biotechnol.* **2000**, *18*, 313–316. (b) Hofmann, R. M.; Cotton, G. J.; Chang, E. J.; Vidal, E.; Veach, D.; Bornmann, W.; Muir, T. W. *Bioorg. Med. Chem. Lett.* **2001**, *11*, 3091–3094. (c) Kurokawa, K.; Mochizuki, N.; Ohba, Y.; Mizuno, H.; Miyawaki, A.; Matsuda, M. *J. Biol. Chem.* **2001**, *276*, 31305–31310. (d) Ting, A. Y.; Kain, K. H.; Klemke, R. L.; Tsien, R. Y. *Proc. Natl. Acad. Sci. U.S.A.* **2001**, *98*, 15003–15008. (e) Sato, M.; Ozawa, T.; Inukai, K.; Asano, T.; Umezawa, Y. *Nat. Biotechnol.* **2002**, *20*, 287–294.

(4) (a) Ohuchi, Y.; Katayama, Y.; Maeda, M. *Analyst* **2000**, *125*, 1905–1907. (b) Ojida, A.; Inoue, M.; Mito-oka, Y.; Hamachi, I. *J. Am. Chem. Soc.* **2003**, *125*, 10184–10185. (c) Ojida, A.; Mito-oka, Y.; Sada, K.; Hamachi, I. *J. Am. Chem. Soc.* **2004**, *126*, 2454–2463.

(5) (a) McIlroy, B. K.; Walters, J. D.; Johnson, J. D. *Anal. Biochem.* **1991**, *195*, 148–152. (b) Post, P. L.; Trybus, K. M.; Taylor, D. L. *J. Biol. Chem.* **1994**, *269*, 12880–12887. (c) Higashi, H.; Sato, K.; Omori, A.; Sekiguchi, M.; Ohtake, A.; Kudo, Y. *NeuroReport* **1996**, *7*, 2695–2700. (d) Higashi, H.; Sato, K.; Ohtake, A.; Omori, A.; Yoshida, S.; Kudo, Y. *FEBS Lett.* **1997**, *414*, 55–60. (e) Yeh, R.-H.; Yan, X.; Cammer, M.; Bresnick, A. R.; Lawrence, D. S. *J. Biol. Chem.* **2002**, *277*, 11527–11532.

[†] JST corporation.

[‡] The University of Tokyo.

[§] Present address: Faculty of Industrial Science and Technology, Tokyo University of Science, Oshamanbe, Hokkaido 049-3514, Japan.

^{*} Present address: Graduate School of Engineering, Osaka University, 2-1 Yamada-oka, Suita City, Osaka 565-0871, Japan.

(1) *Chem. Rev.* **2001**, *101*, issue 8: Protein Phosphorylation and Signaling.

(2) (a) Eisele, F.; Owen, D. J.; Waldmann, H. *Bioorg. Med. Chem.* **1999**, *7*, 193–224. (b) Lawrence, D. S. *Acc. Chem. Res.* **2003**, *36*, 401–409.

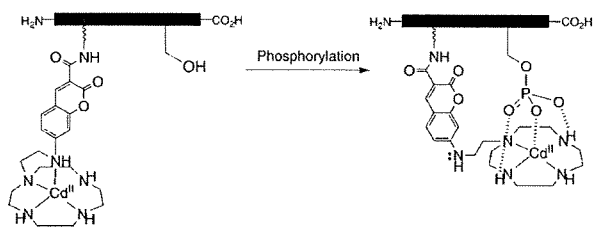
of phosphorylation, and this serves to signal the change of environment upon phosphorylation. The groups of Lawrence and Imperiali have developed chelator-appended fluorescent peptides for monitoring kinase activities.⁶ Upon phosphorylation, these peptides show a significant fluorescence intensity increase owing to the formation of divalent alkaline earth metal complexes coordinated to the newly generated phosphate group and the fluorophore.

Fluorescence measurement at a single wavelength without much shift of either the excitation or emission wavelength can be influenced by artifacts associated with the microscopic imaging system. To reduce the influence of such factors, ratiometric measurement is utilized, namely, simultaneous recording of the fluorescence intensities at two wavelengths and calculation of their ratio.⁷ For this approach, probes that signal phosphorylation via a shift of either excitation or emission wavelength are required.

We have designed a fluorescent anion sensor, consisting of 7-aminotrifluoromethylcoumarin as a fluorescent reporter and Cd^{II}-cyclen (1,4,7,10-tetraazacyclododecane) as an anion host.⁸ This sensor molecule can detect phosphate anion species, such as pyrophosphate, with high sensitivity in aqueous neutral solution. As an extension of the anion sensor concept, we have newly designed an anion sensor-appended peptide substrate for protein kinases. Here we describe the sensing of a kinase-mediated phosphorylation event by a fluorescent peptide sensor. This novel class of peptide probe exhibited a shift of excitation spectrum upon phosphorylation, enabling ratiometric measurement of kinase activity. This technique can provide more precise data than measurement at a single wavelength, canceling out the influence of variations in instrument efficiency, content of effective dye, and so forth.

The operational concept of the peptide sensor is schematically presented in Scheme 1. This peptide sensor consists of

Scheme 1. Schematic Representation of our Peptide Sensor for Phosphorylation



an anion sensor and a phosphorylation target peptide sequence. The sensing moiety is positioned near the target hydroxyl amino acid residue. In neutral aqueous solution,

(6) (a) Chen, C. A.; Yeh, R. H.; Lawrence, D. S. *J. Am. Chem. Soc.* **2002**, *124*, 3840–3841. (b) Shults, M. D.; Imperiali, B. *J. Am. Chem. Soc.* **2003**, *125*, 14248–14249.

(7) (a) Tsien, R. Y.; Harootyan, A. T. *Cell Calcium* **1990**, *11*, 93. (b) Kikuchi, K.; Takakusa, H.; Nagano, T. *Trends in Anal. Chem.* **2004**, *23*, 407–415.

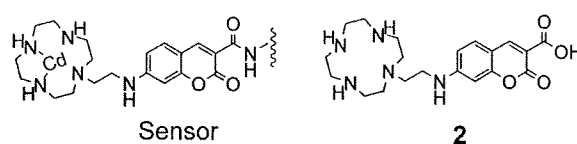
(8) Mizukami, S.; Nagano, T.; Urano, Y.; Odani, A.; Kikuchi, K. *J. Am. Chem. Soc.* **2002**, *124*, 3920–3925.

Cd^{II} of the cyclen complex is coordinated by the four nitrogen atoms of cyclen and the aromatic 7-amino group of coumarin.⁹ When a negatively charged phosphate group coordinates to Cd^{II} as the fifth ligand, the aromatic 7-amino group is displaced from the metal. The anion sensor signals this replacement, because the increase of electron density of the 7-amino group induces a red shift of the excitation spectrum. We have designed peptide sensor **1** for protein kinase A (PKA) as shown in Scheme 2. The sequence of the peptide

Scheme 2. Sequence of Peptide Sensor and its Phosphorylated Standard Employed in This Study

Sensor-(CH₂)₅-LRRASLG-CONH₂ **1**

Sensor-(CH₂)₅-LRRApSLG-CONH₂ **1P**



sensor is known as Kemptide and has been shown to be a good substrate for the kinase.¹⁰ The sensing moiety is positioned at the N-terminus of the peptide through an alkyl tether, enabling recognition of a phosphorylated serine residue. We also designed a phosphorylated sensor **1P** to estimate preliminarily the extent of spectral change upon phosphorylation.

The cyclen-appended 7-aminocoumarincarboxylic acid **2** was synthesized according to the established procedure.⁸ The peptide sequence was synthesized using Fmoc solid-phase chemistry on an automated peptide synthesizer and the ligand **2** was manually coupled to the amino linker. The resulting peptide conjugate was metalated with Cd(ClO₄)₂ to give the desired peptide sensor **1**. Phosphorylated peptide sensor **1P** was prepared by protein kinase-mediated phosphorylation of the peptide conjugate followed by metalation with Cd^{II}. The structures of **1** and **1P** were confirmed by MALDI-TOF MS (matrix assisted laser desorption/ionization-time-of-flight mass spectrometry) and quantitative amino acid analysis.

We tested the sensing ability of peptide sensor **1** by comparing the excitation spectrum with that of the phosphorylated product, **1P** (see Supporting Information). Upon phosphorylation, the excitation intensity at 360 nm decreased, whereas the intensity at 410 nm increased. The ratio of the excitation intensities (410 nm/360 nm) changed

(9) (a) Koike, T.; Watanabe, T.; Aoki, S.; Kimura, E.; Shiro, M. *J. Am. Chem. Soc.* **1996**, *118*, 12696–12703. (b) Aoki, S.; Kaido, S.; Fujioka, H.; Kimura, E. *Inorg. Chem.* **2003**, *42*, 1023–1030.

(10) (a) Kemp, B. E.; Graves, D. J.; Benjamini, E.; Krebs, E. G. *J. Biol. Chem.* **1977**, *252*, 4888–4894. (b) Kemp, B. E. *J. Biol. Chem.* **1980**, *255*, 2914–2918.

1.8-fold (from a value of 0.54 to 0.96), demonstrating that peptide phosphorylation can be detected with an anion sensor.¹¹

To investigate the utility of the compound as a fluorescent probe for protein kinases, we measured the time-dependent change of the excitation spectrum of **1** treated with ATP (adenosine 5'-triphosphate) and PKA catalytic subunit (Figure 1). The phosphorylation reaction

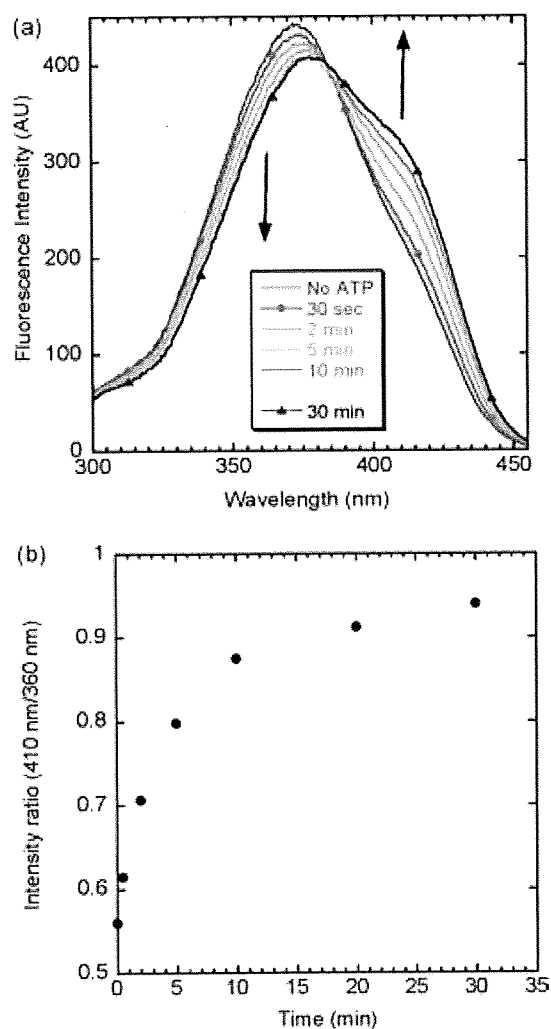


Figure 1. (a) Time course of the excitation spectra of **1** treated with PKA catalytic subunit. The peptide sensor **1** (1.3 μ M) was incubated in 50 mM HEPES (pH 7.4), 5 mM Mg(OAc)₂ containing 4.3 nM catalytic subunit and 3.3 μ M ATP at 23 \pm 0.1 $^{\circ}$ C. (b) Plot of intensity ratio (410 nm/360 nm) versus reaction time.

was initiated by the addition of ATP to a mixture of **1** and the catalytic subunit. Though ATP strongly coordinates to the Cd^{II} complex of the anion sensor, addition of

(11) A significant shift of the absorption peak was also observed for the Cd^{II} complex of methylated compound **2** upon addition of pyrophosphate anion. Titration of the complex with pyrophosphate gave the K_d value of 53 μ M.

this organic polyanion had no significant effect on the excitation spectrum under the conditions employed.¹² As can be seen from Figure 1, the excitation spectra of **1** changed ratiometrically; the intensity at 360 nm decreased with a concomitant intensity increase at 410 nm. The ratio of excitation intensity (410 nm/360 nm) increased 1.7 fold after 30 min reaction time, and this is similar to the value obtained by comparison of the excitation spectra of authentic **1** and **1P**. The phosphorylation reaction was accelerated by increasing the quantity of kinase employed for the reaction (see Supporting Information).

We further carried out an inhibition experiment using the heat-stable inhibitor protein of PKA (PKI), which acts competitively with respect to the phosphoryl-accepting substrate (Figure 2).¹³ Dose-dependent inhibition of kinase

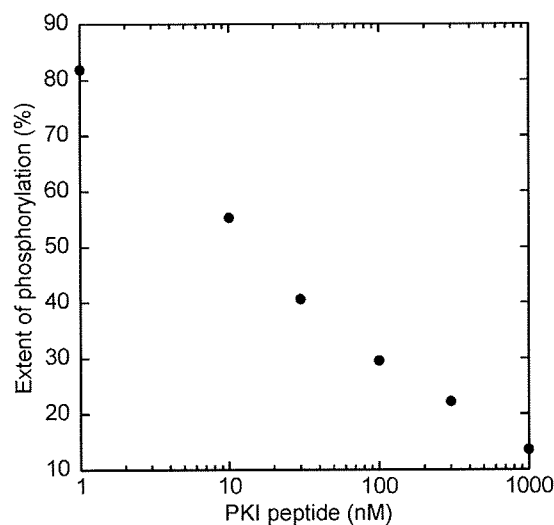


Figure 2. Titration of PKA-mediated phosphorylation of **1** with PKI peptide. The phosphorylation reaction was carried out in 50 mM HEPES (pH 7.4), 5 mM Mg(OAc)₂ containing 1.0 μ M **1**, 4.3 nM catalytic subunit, 3.3 μ M ATP and various amounts of PKI peptide at 23 \pm 0.1 $^{\circ}$ C. Extent of phosphorylation (%) was determined by comparing the intensity ratio increase at the early phase of the reaction (0–5 min) with that of the control.

activity by PKI peptide was observed for phosphorylation of **1** with an IC₅₀ (half maximal inhibitory concentration) of ca. 15 nM under the conditions employed. This result indicates that the ratiometric spectral change is caused by PKA-mediated phosphorylation of **1**.¹⁴

In conclusion, we have developed a new fluorescent probe for protein kinase based on the anion sensing principle. It has been demonstrated that this peptide probe can be used

(12) The addition of more than three equivalents of ATP to the peptide sensor **1** induced an excitation change at two wavelength (360 and 410 nm), which indicates the coordination of ATP to the metal complex moiety.

(13) (a) Cheng, H. C.; Kemp, B. E.; Pearson, R. B.; Smith, A. J.; Misconi, L.; Van Patten, S. M.; Walsh, D. A. *J. Biol. Chem.* **1986**, *261*, 989–992. (b) Glass, D. B.; Cheng, H. C.; Mueller, L. M.; Reed, J.; Walsh, D. A. *J. Biol. Chem.* **1989**, *264*, 8802–8810.

to continuously monitor kinase-mediated phosphorylation through intensity measurements at two wavelengths. This peptide sensor might serve as the basis for a range of anion sensor-based phosphorylation probes for many different protein kinases.

(14) Actual phosphorylation of peptide sensor **1** was confirmed by analyzing the reaction mixture, using C₁₈ reverse-phase HPLC (high-performance liquid chromatography). Time-dependent production of phosphorylated product was observed when the sensor **1** was exposed to PKA catalytic subunit. The phosphorylated product co-eluted with authentic standard **1P** from the HPLC column.

Acknowledgment. We thank Prof. H. Mihara and Dr. T. Takahashi at the Tokyo Institute of Technology for technical assistance in peptide synthesis.

Supporting Information Available: Synthesis of anion sensor and peptide conjugate, fluorescence experiment, protein kinase assay. This material is available free of charge via the Internet at <http://pubs.acs.org>.

OL9006508

Design and Synthesis of Coumarin-Based Zn²⁺ Probes for Ratiometric Fluorescence Imaging

Shin Mizukami, Satoshi Okada, Satoshi Kimura, and Kazuya Kikuchi*

Division of Advanced Science and Biotechnology, Graduate School of Engineering, Osaka University,
2-1 Yamadaoka, Suita, Osaka 565-0871, Japan

Received February 5, 2009

The physiological roles of free Zn²⁺ have attracted great attention. To clarify those roles, there has been a need for ratiometric fluorescent Zn²⁺ probes for practical use. We report the rational design and synthesis of a series of ratiometric fluorescent Zn²⁺ probes. The structures of the probes are based on the 7-hydroxycoumarin structure. We focused on the relationship between the electron-donating ability of the 7-hydroxy group and the excitation spectra of 7-hydroxycoumarins, and exploited that relationship in the design of the ratiometric probes; as a result, most of the synthesized probes showed ratiometric Zn²⁺-sensing properties. Then, we designed and synthesized ratiometric Zn²⁺ probes that can be excited with visible light, by choosing adequate substituents on coumarin dyes. Since one of the probes could permeate living cell membranes, we introduced the probe to living RAW264 cells and observed the intracellular Zn²⁺ concentration via ratiometric fluorescence microscopy. As a result, the ratio value of the probe changed quickly in response to intracellular Zn²⁺ concentration.

Introduction

Zinc is one of the most heavily studied metals in biology. The biological roles of Zn²⁺ have been studied since the 1940s; the main studies focused on its biochemical roles, either as structural elements in enzymes and transcription factors or as the catalytic elements in enzymatic activity centers.¹ These Zn²⁺s are thought to be bound strongly to peptides or proteins. Meanwhile, the physiological roles of free Zn²⁺ have recently attracted great attention, mainly in neurology.² Generally, to study the physiological roles of biomolecules in living cells or tissues, it is quite useful to visualize them under microscopes; fluorescent probes are useful in this endeavor. For example, rapid progress in physiological Ca²⁺ studies has been accomplished through the use of fluorescent Ca²⁺ probes such as fura-2, fluo-3, and succeeding compounds.³ The success of Ca²⁺ probes has, in turn, encouraged the development of fluorescent probes for other various biomolecules.

With regards to fluorescent probes for Zn²⁺,⁴ the pioneering compound was TSQ (*N*-(6-methoxy-8-quinolyl)-*p*-toluene-

sulfonamide), as reported by Frederickson et al.⁵ Although it was difficult for TSQ to be applied to live cell imaging for hydrophobicity, its hydrophilic derivative, Zinquin, enabled the fluorescence microscopic imaging of free Zn²⁺.⁶ Such quinoline-based probes are, however, excited by ultraviolet light, thus inducing cell damage and autofluorescence from fluorescent biomolecules such as flavin derivatives. Thus, the fluorescent probes for longer-wavelength excitation have been actively developed by several groups.^{7–10} Since most of these probes are fluorescein-based, they are much brighter than

*To whom correspondence should be addressed. E-mail: kkikuchi@mls.eng.osaka-u.ac.jp.

(1) (a) Prasad, A. S. *Biochemistry of Zinc*; Plenum Press: New York, 1993.

(b) Vallee, B. L.; Falchuk, K. H. *Physiol. Rev.* 1993, 73, 79–118.

(2) Frederickson, C. J.; Koh, J. -Y.; Bush, A. I. *Nat. Rev. Neurosci.* 2005, 6, 449–462.

(3) Kao, J. P. Y. *Methods Cell Biol.* 1994, 40, 155–181.

(4) See following reviews: (a) Burdette, S. C.; Lippard, S. J. *Coord. Chem. Rev.* 2001, 216–217, 333–361. (b) Kimura, E.; Aoki, S. *Biometals* 2001, 14, 191–204. (c) Kikuchi, K.; Komatsu, K.; Nagano, T. *Curr. Opin. Chem. Biol.* 2004, 8, 182–191. (d) Dai, Z.; Canary, J. W. *New J. Chem.* 2007, 31, 1708–1718.

(5) Frederickson, C. J.; Kasarskis, E. J.; Ringo, D.; Frederickson, R. E. *J. Neurosci. Methods* 1987, 20, 91–103.

(6) Zalewski, P. D.; Forbes, I. J.; Betts, W. H. *Biochem. J.* 1993, 296, 403–408.

(7) (a) Hirano, T.; Kikuchi, K.; Urano, Y.; Higuchi, T.; Nagano, T. *Angew. Chem., Int. Ed.* 2000, 39, 1052–1054. (b) Hirano, T.; Kikuchi, K.; Urano, Y.; Higuchi, T.; Nagano, T. *J. Am. Chem. Soc.* 2000, 122, 12399–12400. (c) Hirano, T.; Kikuchi, K.; Urano, Y.; Nagano, T. *J. Am. Chem. Soc.* 2002, 124, 6555–6562. (d) Komatsu, K.; Kikuchi, K.; Kojima, H.; Urano, Y.; Nagano, T. *J. Am. Chem. Soc.* 2005, 127, 10197–10204.

(8) (a) Walkup, G. K.; Burdette, S. C.; Lippard, S. J.; Tsien, R. Y. *J. Am. Chem. Soc.* 2000, 122, 5644–5645. (b) Burdette, S. C.; Walkup, G. K.; Spingler, B.; Tsien, R. Y.; Lippard, S. J. *J. Am. Chem. Soc.* 2001, 123, 7831–7841. (c) Burdette, S. C.; Frederickson, C. J.; Bu, W.; Lippard, S. J. *J. Am. Chem. Soc.* 2003, 125, 1778–1787. (d) Chang, C. J.; Nolan, E. M.; Jaworski, J.; Burdette, S. C.; Sheng, M.; Lippard, S. J. *Chem. Biol.* 2004, 11, 203–210. (e) Nolan, E. M.; Lippard, S. J. *Inorg. Chem.* 2004, 43, 8310–8317. (f) Nolan, E. M.; Jaworski, J.; Okamoto, K. -I.; Hayashi, Y.; Sheng, M.; Lippard, S. J. *J. Am. Chem. Soc.* 2005, 127, 16812–16823. (g) Nolan, E. M.; Jaworski, J.; Racine, M. E.; Sheng, M.; Lippard, S. J. *Inorg. Chem.* 2006, 45, 9748–9757. (h) Nolan, E. M.; Ryu, J. W.; Jaworski, J.; Feazell, R. P.; Sheng, M.; Lippard, S. J. *J. Am. Chem. Soc.* 2006, 128, 15517–15528.

(9) Gee, K. R.; Zhou, Z. -L.; Qian, W. -J.; Kennedy, R. *J. Am. Chem. Soc.* 2002, 124, 776–778.

(10) Tang, B.; Huang, H.; Xu, K. H.; Tong, L. L.; Yang, G. W.; Liu, X.; An, L. *G. Chem. Commun.* 2006, 3609–3611.

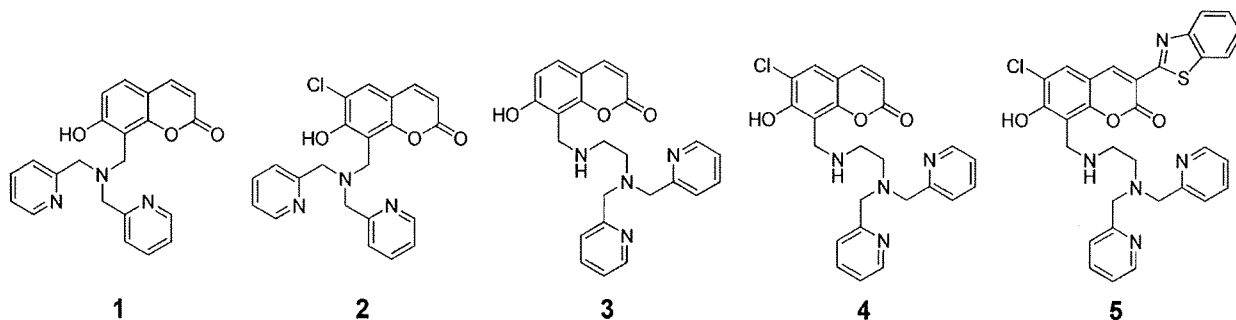


Figure 1. Structures of synthesized probes.

quinoline-based probes. Although such higher-intensity probes have several biological applications,¹¹ they suffer from a dependence on fluorescence intensity, in terms of dye localization or the intensity of the excitation light.

In the course of overcoming these drawbacks, ratiometric fluorescent probes for Zn^{2+} ions have been a recent focus.¹² Although there have been several ratiometric Zn^{2+} probes reported,¹³ few can be practically used; in many cases, there are problems with short-wavelength excitation, low fluorescence intensity, low hydrophilicity, or elsewhere. Thus, we started developing ratiometric fluorescent Zn^{2+} probes for practical use in biological experiments.

We focused on coumarin as the fundamental platform of the fluorescent probes. Coumarins are known to be strongly fluorescent compounds, and it is easy to synthesize coumarin derivatives in general. For these reasons, coumarin-based probes are widely used in various biological assays.¹⁴ In the case of fluorescence imaging, a coumarin-based fluorescent probe BTC is utilized for detecting Ca^{2+} in living cells.¹⁵ Concerning Zn^{2+} -sensing probes, there have been several reports about coumarin-based fluorescent probes.¹⁶ Brückner et al. reported of a ratiometric coumarin-based probe; however, the ratiometric property was achieved only in organic solvent.^{16a,16b} In the case of other ratiometric probes, the metal selectivity and/or the cellular application was not demonstrated. Thus, there are currently no practical

ratiometric Zn^{2+} probes based on a coumarin structure. Although recently Nagano et al. reported of a ratiometric probe based on an iminocoumarin structure,^{13f} an iminocoumarin structure is potentially labile against hydrolysis. Therefore, there is still a great demand for ratiometric Zn^{2+} probes that can be used in imaging. We report here the design, synthesis, and photophysical properties of a series of ratiometric fluorescent Zn^{2+} probes based on a 7-hydroxy-coumarin structure, after having investigated the cell membrane permeability and the ability to use Zn^{2+} in the ratiometric fluorescence imaging of living cells.

Results

Synthesis of Probes. First, we designed and synthesized a prototypical probe **1**, in only one step, from commercial compounds by using a Mannich-type reaction (Figure 1). We also designed and synthesized probes **2–5** by changing the ligand structure or substituting a coumarin structure (Figure 1). In the case of probe **2**, we introduced a chlorine atom at the 6-position for decreasing the pK_a of the 7-hydroxy group. In probe **3**, the ligand structure was modified; this substitution was expected to affect both the Zn^{2+} -binding affinity and the pK_a of the 7-hydroxy group. In probe **4**, we expected a cooperative effect from the introduced chlorine atom and the change in ligand structure. In probe **5**, a further substitution of a benzothiazolyl group was given at the 3-position of **4**. 3-Benzothiazolylcoumarin is the basic structure of a ratiometric Ca^{2+} probe BTC,¹⁵ which can be excited with visible light; it is already in practical use. Thus, **5** was expected to be excited at the visible wavelength. Detailed synthesis schemes and procedures are described in the Supporting Information section.

Photophysical Properties of Probes. The excitation, emission, and absorption spectra of the prototypical probe **1** were measured (Figures 2(a), 3(a), and Supporting Information, Figure S1(a), respectively). The absorption spectra shifted toward longer wavelengths with the addition of Zn^{2+} , in a concentration-dependent manner. The peak top shifted from 331 to 357 nm. The maximum excitation wavelength also shifted with the addition of Zn^{2+} , and the fluorescence intensity largely increased. The emission spectra scarcely shifted ($\lambda_{max} \approx 450$ nm) because of the Zn^{2+} addition.

Meanwhile, the absorption and excitation spectra of the 6-chlorinated probe **2** showed a blue shift (λ_{ex} : 368 nm \rightarrow 362 nm, λ_{abs} : 367 nm \rightarrow 360 nm) with the addition of Zn^{2+} (Figures 2(b) and Supporting Information, Figure S1(b)). The emission spectra also slightly shifted toward

(11) (a) Ueno, S.; Tsukamoto, M.; Hirano, T.; Kikuchi, K.; Yamada M. K.; Nishiyama, N.; Nagano, T.; Matsuki, N.; Ikegaya, Y. *J. Cell Biol.* **2002**, *158*, 215–220. (b) Qian, J.; Noebels, J. L. *J. Physiol.* **2005**, *566*, 747–758. (c) Yamasaki, S.; Sakata-Sogawa, K.; Hasegawa, A.; Suzuki, T.; Kabu, K.; Sato, E.; Kurosaki, T.; Yamashita, S.; Tokunaga, M.; Nishida, K.; Hirano, T. *J. Cell Biol.* **2007**, *177*, 637–645.

(12) See the following review: Carol, P.; Sreejith, S.; Ajayaghosh, A. *Chem. Asian J.* **2007**, *2*, 338–348.

(13) (a) Maruyama, S.; Kikuchi, K.; Hirano, T.; Urano, Y.; Nagano, T. *J. Am. Chem. Soc.* **2002**, *124*, 10650–10651. (b) Woodrooffe, C. C.; Lippard, S. J. *J. Am. Chem. Soc.* **2003**, *125*, 11458–11459. (c) Chang, C. J.; Jaworski, J.; Nolan, E. M.; Sheng, M.; Lippard, S. J. *Proc. Natl. Acad. Sci. U.S.A.* **2004**, *101*, 1129–1134. (d) Taki, M.; Wolford, J. L.; O'Halloran, T. V. *J. Am. Chem. Soc.* **2004**, *126*, 712–713. (e) Kiyose, K.; Kojima, H.; Urano, Y.; Nagano, T. *J. Am. Chem. Soc.* **2006**, *128*, 6548–6549. (f) Komatsu, K.; Urano, Y.; Kojima, H.; Nagano, T. *J. Am. Chem. Soc.* **2007**, *129*, 13447–13454. (g) Zhang, Y.; Guo, X.; Si, W.; Jia, L.; Qian, X. *Org. Lett.* **2008**, *10*, 473–476. (h) Taki, M.; Watanabe, Y.; Yamamoto, Y. *Tetrahedron Lett.* **2009**, *50*, 1345–1347.

(14) (a) Goddard, J. P.; Raymond, J. L. *Trends Biotechnol.* **2004**, *22*, 363–370. (b) Katerinopoulos, H. E. *Curr. Pharm. Des.* **2004**, *10*, 3835–3852.

(15) Itaridou, H.; Foukaraki, E.; Kuhn, M. A.; Marcus, E. M.; Haugland, R. P.; Katerinopoulos, H. E. *Cell Calcium* **1994**, *15*, 190–198.

(16) (a) Lim, N. C.; Brückner, C. *Chem. Commun.* **2004**, 1094–1095. (b) Lim, N. C.; Schuster, J. V.; Porto, M. C.; Tanudra, M. A.; Yao, L.; Freake, H. C.; Brückner, C. *Inorg. Chem.* **2005**, *44*, 2018–2030. (c) Dakanali, M.; Roussakis, E.; Kay, A. R.; Katerinopoulos, H. E. *Tetrahedron Lett.* **2005**, *45*, 4193–4196. (d) Kulatilake, C. P.; de Silva, S. A.; Eliav, Y. *Polyhedron* **2006**, *25*, 2593–2596. (e) Zhang, L.; Dong, S.; Zhu, L. *Chem. Commun.* **2007**, 1891–1893.

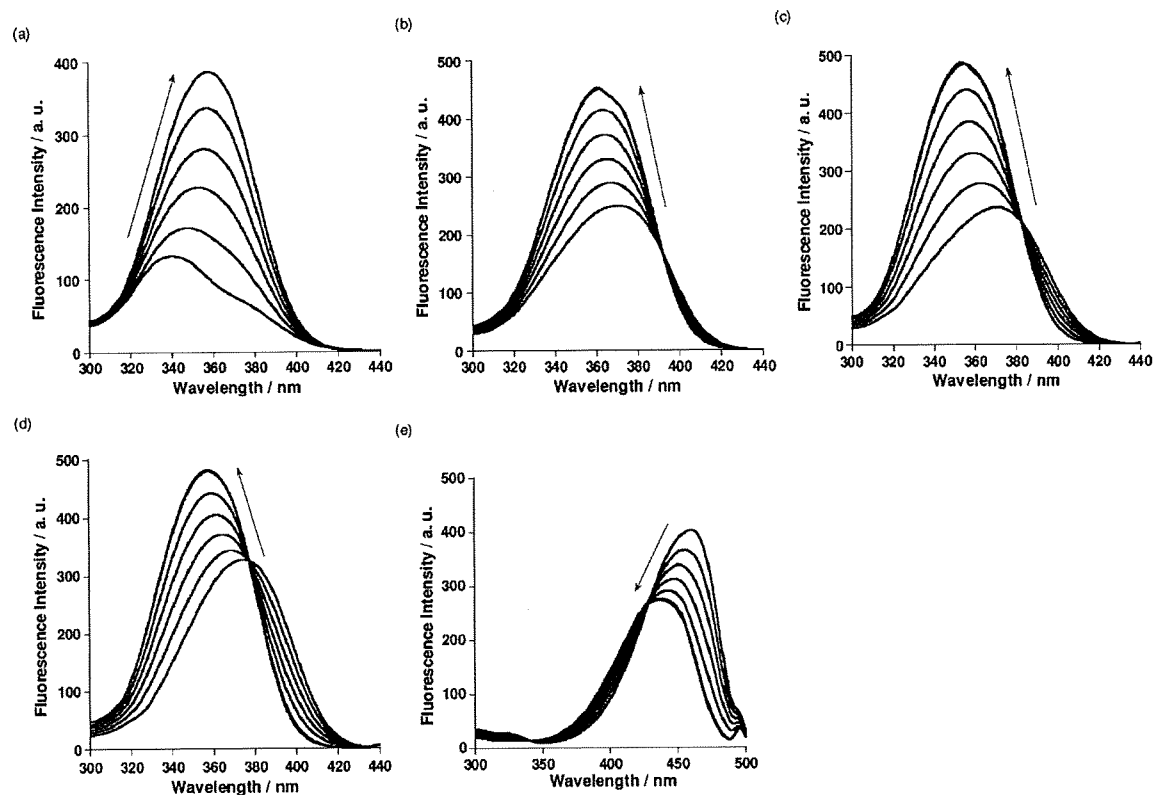


Figure 2. Excitation spectra of (a) $5 \mu\text{M}$ **1** ($\lambda_{\text{em}} = 450 \text{ nm}$), (b) $5 \mu\text{M}$ **2** ($\lambda_{\text{em}} = 445 \text{ nm}$), (c) $5 \mu\text{M}$ **3** ($\lambda_{\text{em}} = 440 \text{ nm}$), (d) $5 \mu\text{M}$ **4** ($\lambda_{\text{em}} = 443 \text{ nm}$), and (e) $1 \mu\text{M}$ **5** ($\lambda_{\text{em}} = 494 \text{ nm}$), in the presence of various concentrations of Zn^{2+} (0, 0.2, 0.4, 0.6, 0.8, and 1.0 equiv to the probe concentration) in 100 mM HEPES buffer solution (pH 7.4). Arrows indicate the directions of the spectral changes as Zn^{2+} concentration increased.

shorter wavelengths, because of the Zn^{2+} addition (Figure 3(b)). The excitation, emission, and absorption spectra of **3–5** also showed blue shifts on account of adding Zn^{2+} (Figures 2(c)–(e), 3(c)–(e), and Supporting Information, Figure S1(c)–(e)).

We also investigated the fluorescence quantum yields of the synthesized compounds in the free form versus the Zn^{2+} complex form. The fluorescence quantum yields of probes **1–4** were increased by complexation with Zn^{2+} ; all but **5** showed a remarkable change in fluorescence quantum yield. The photophysical data for the synthesized probes are summarized in Table 1.

Effect of pH on Photophysical Properties of Probes. We investigated the effect of solution pH on the photophysical properties of the synthesized probes. The absorption spectra of **1** at various solution pHs are shown in Figure 4(a). In acidic solution, the maximum absorption wavelength was at around 326 nm; in basic solution, however, the peak top shifted to 377 nm. In the case of probes **2–5**, their absorption spectra also showed red shifts as solution pH increased (Supporting Information, Figure S2).

Next, the effect of pH on the excitation spectrum of **1** was investigated. The fluorescence spectra of **1** at various solution pHs are shown in Figure 4(b). When the solution pH was increased from an acidic value, the fluorescence intensity increased; this trend continued until the pH was neutral, and the intensity then decreased when the pH was in excess of 8.

The fluorescence intensity of probes **1–5** at several solution pH points are plotted in Figure 4(c). Concerning

all synthesized probes, the fluorescence intensity values decreased in the acidic and basic regions, although a control compound—7-hydroxy-8-methylcoumarin (HMC), which lacks a DPA ligand—did not show a fluorescence decrease at a basic-solution pH. Most probes, with the exception of **2**, showed virtually no physiological pH-sensitivity in the pH region of 7.4. The $\text{p}K_{\text{a}}$ values of probes **1–5** were determined by pH titrating absorption measurements (Table 1). We also carried out potentiometric titration experiments (Supporting Information, Figure S5). For each compound, the $\text{p}K_{\text{a}}$ value determined by absorbance titration was roughly consistent with one of the $\text{p}K_{\text{a}}$ values determined by potentiometric titration (Supporting Information, Table S1).

Metal-Binding Properties. (1). **Stoichiometry of Binding to Zn^{2+} .** The binding stoichiometry of the probes to Zn^{2+} was investigated by Job's plot.¹⁷ It was confirmed that all probes form 1:1 complexes with Zn^{2+} (Supporting Information, Figure S3).

(2). **Apparent Binding Constants to Zn^{2+} .** The apparent dissociation constants (K_{d}) of probes **1–5** in neutral aqueous buffer were determined by plotting the fluorescence intensity to free Zn^{2+} concentration (Supporting Information, Figure S4). The K_{d} values of probes **1–5** were in the range of 3.6–28 pM, as shown in Table 1.

(3). **Metal-Sensing Selectivity.** We investigated the fluorescence ratio values of the probes in response to various metal ions (Figure 5). The results of probes **1–4**

(17) Job, P. *Ann. Chim.* 1928, 9, 113–203.

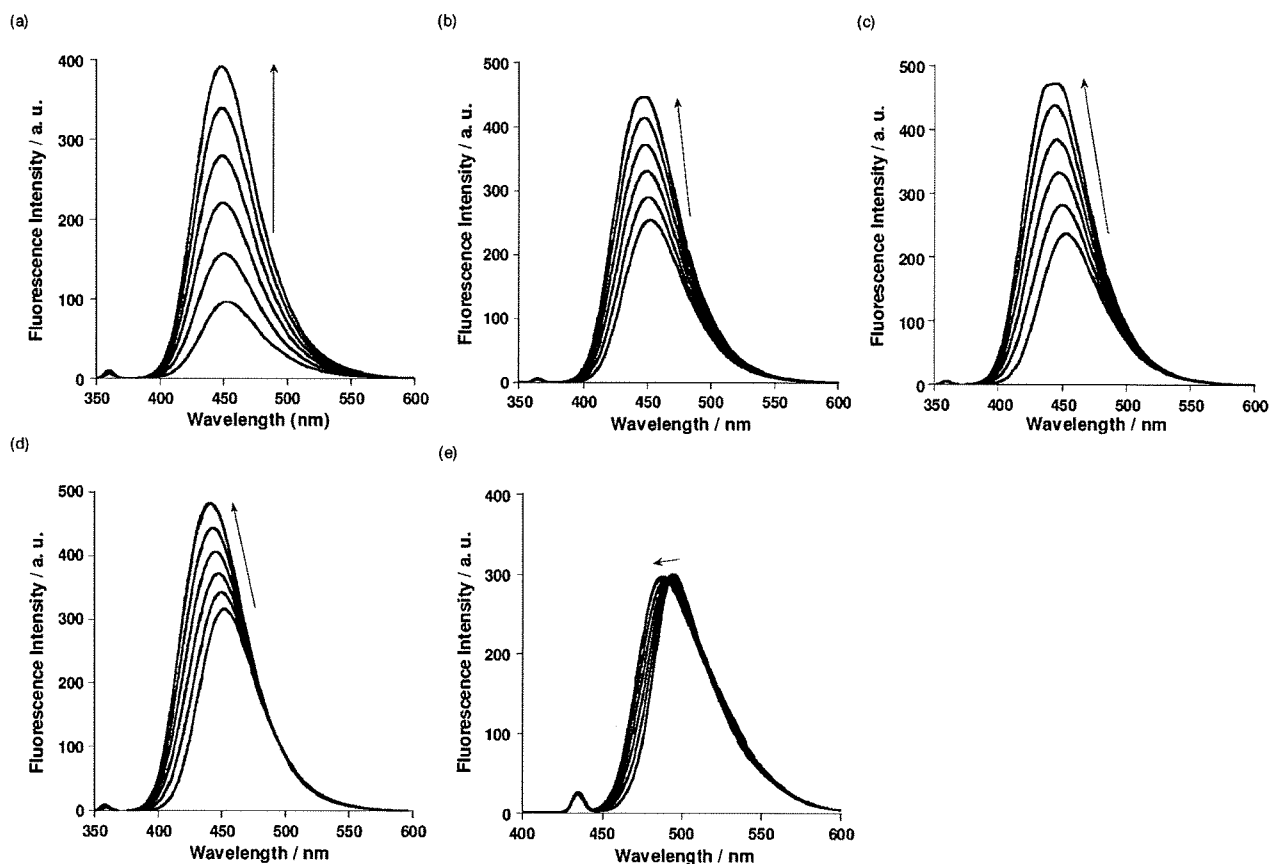


Figure 3. Emission spectra of (a) $5 \mu\text{M}$ **1** ($\lambda_{\text{ex}} = 358 \text{ nm}$), (b) $5 \mu\text{M}$ **2** ($\lambda_{\text{ex}} = 362 \text{ nm}$), (c) $5 \mu\text{M}$ **3** ($\lambda_{\text{ex}} = 357 \text{ nm}$), (d) $5 \mu\text{M}$ **4** ($\lambda_{\text{ex}} = 357 \text{ nm}$), and (e) $1 \mu\text{M}$ **5** ($\lambda_{\text{ex}} = 432 \text{ nm}$), in the presence of various concentrations of Zn^{2+} (0, 0.2, 0.4, 0.6, 0.8, and 1.0 equiv to the probe concentration) in 100 mM HEPES buffer solution (pH 7.4). Arrows indicate the directions of the spectral changes as Zn^{2+} concentration increased.

Table 1. Physical Properties of Synthesized Probes

compound	absorption				excitation		emission		quantum yield		dissociation constant to Zn^{2+}	
	$\lambda_{\text{max}}/\text{nm}$ $\epsilon/\text{M}^{-1} \text{cm}^{-1}$				$\lambda_{\text{max}}/\text{nm}$		$\lambda_{\text{max}}/\text{nm}$		Φ		K_d/pM	$\text{p}K_a^a$
	free		Zn^{2+}		free	Zn^{2+}	free	Zn^{2+}	free	Zn^{2+}		
1	331	12,300	357	16,500	344	358	451	450	0.41	0.66	28	8.9
2	367	15,100	360	17,600	368	362	450	445	0.51	0.71	14	4.0
3	369	14,100	351	18,000	374	357	452	443	0.46	0.83	5.2	6.3
4	372	19,700	354	19,100	374	357	450	440	0.52	0.80	5.0	3.7
5	442	51,500	423	48,500	454	432	494	487	>0.96	>0.99	3.6	2.5

^a $\text{p}K_a$ values determined by absorbance titration.

were quite similar to those of other probes that have a dipicolylamino group as the ligand. The fluorescence ratio values of all compounds were not affected by physiologically abundant metal ions such as Na^+ , K^+ , Mg^{2+} , or Ca^{2+} , even when the concentration of those metal ions were 5 mM —although Cd^{2+} also changed the fluorescence spectra. Regarding transition metals, Fe^{3+} , Co^{2+} , Ni^{2+} , and Cu^{2+} caused a quenching of the fluorescence.

Ratiometric Zn^{2+} Imaging in Living Cells. For the biological application, we first investigated cell permeability. RAW264 cells were incubated with our synthesized probes; of the five probes, only **5** successfully permeated the cells (Figure 6(a)). The ratiometric fluorescence images of the same picture as in Figure 6(a) were

shown in Figure 6(b) top, where the cells were excited at two excitation wavelengths, 380 and 450 nm; the fluorescence ratio values were calculated with imaging software. Next, we investigated the Zn^{2+} -sensing ability of **5** in living cells. A total of $5 \mu\text{M}$ pyrithione as a Zn^{2+} ionophore and $50 \mu\text{M}$ Zn^{2+} were added to the cells, to increase the intracellular Zn^{2+} concentration $[\text{Zn}^{2+}]_i$. The ratio fluorescence values (F_{380}/F_{450}) were increased gradually, and became constant within several minutes; the pseudocolor changed purple or blue to yellow or green, which means the increase of the ratio fluorescence values (Figure 6(b) middle). Then, $100 \mu\text{M}$ TPEN (N,N,N',N' -tetrakis(2-pyridylmethyl)ethylenediamine) was added, to decrease free $[\text{Zn}^{2+}]_i$ by chelating Zn^{2+} . The ratio fluorescence values were decreased to the background level with

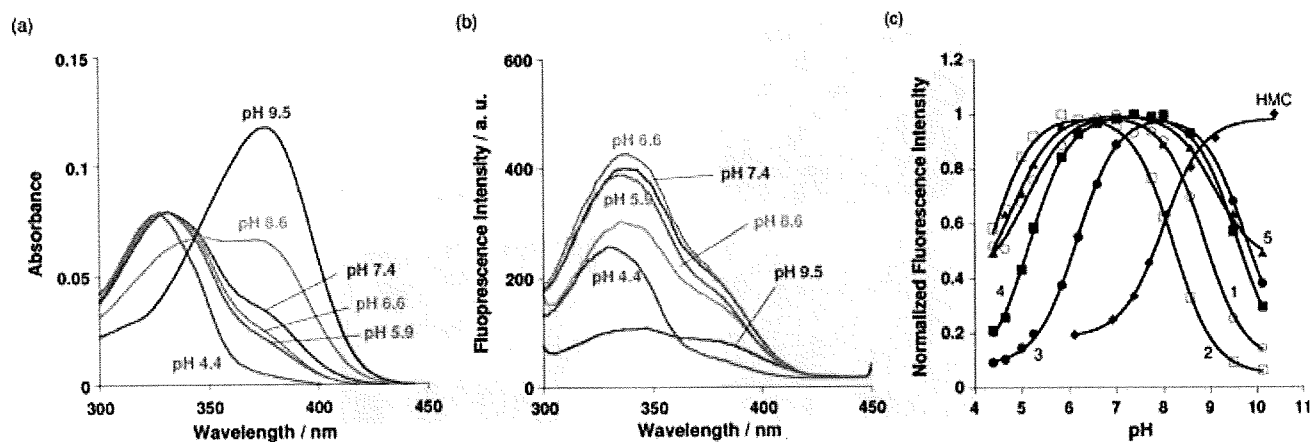


Figure 4. (a) Absorption and (b) excitation spectra ($\lambda_{em} = 451$ nm) of **1** at various solution pHs. (c) Effect of pH on fluorescence intensity of synthesized probes.

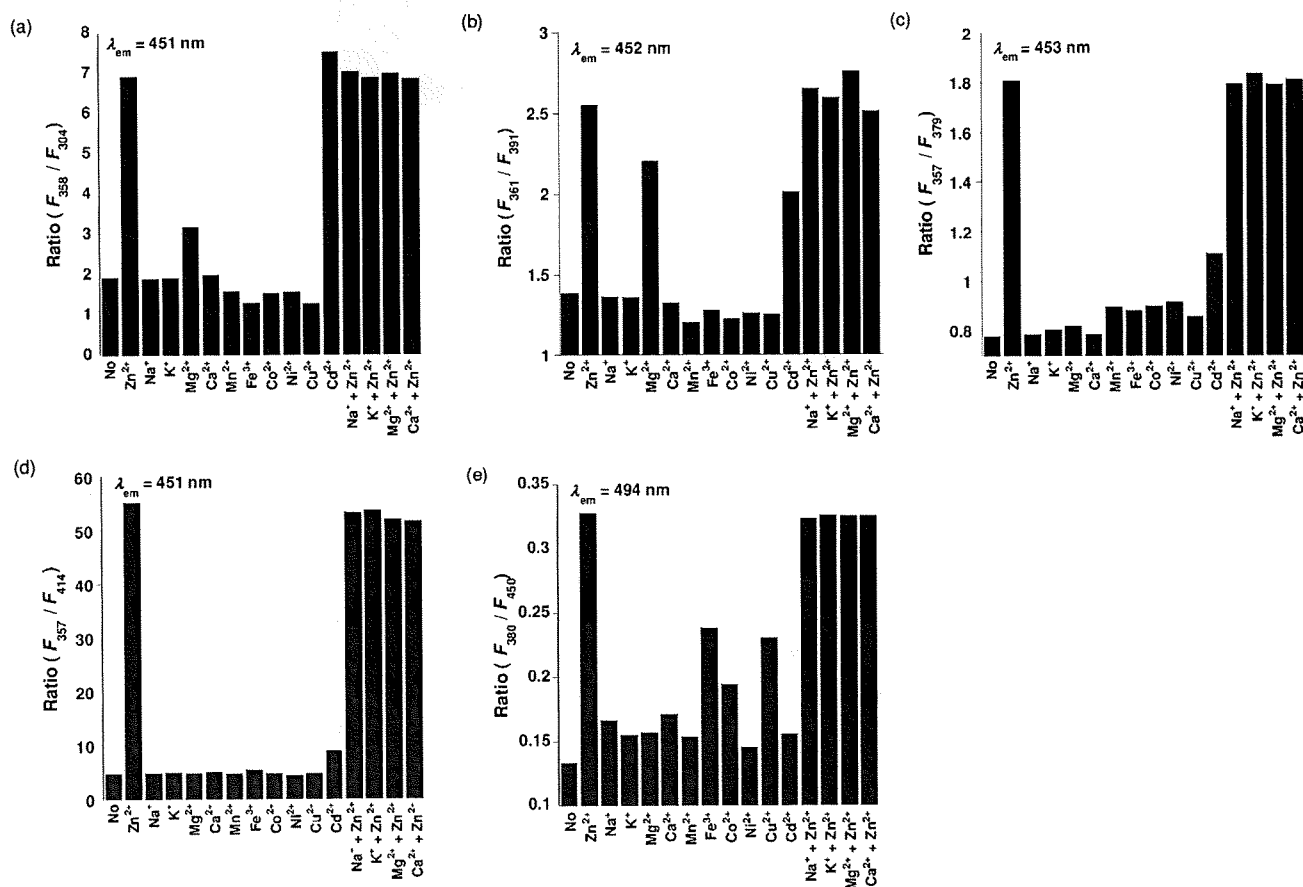


Figure 5. Metal-sensing selectivity of compounds (a) **1**, (b) **2**, (c) **3**, (d) **4**, and (e) **5**. F_x : fluorescence intensity excited at x nm. Na^+ , K^+ , Mg^{2+} , and Ca^{2+} were added at 1,000 times the concentration of the probes. Zn^{2+} , Mn^{2+} , Fe^{3+} , Ni^{2+} , Co^{2+} , Cu^{2+} , and Cd^{2+} were added at the equivalent concentration of the probes.

the pseudocolor getting back to the initial color (Figure 6(b) bottom). The time course of the fluorescence ratio values in three different areas indicated in Figure 6(a) were shown in Figure 6(c).

Discussion

Design of Prototypical Probe 1. First, we designed **1** as a prototypical compound of coumarin-based ratiometric

Zn^{2+} probes (Figure 1). As the chromophore, we chose 7-hydroxycoumarin, also called umbelliferone, because of its strong fluorescence intensity and easy synthesis. As the metal ligand, a dipicolylamine (DPA) structure was chosen because of its high specificity, high stability, and fast complexation ability with Zn^{2+} . Although coumarin-based Zn^{2+} probes with a DPA ligand have been reported,^{16b,16d} they did not exhibit ratiometric fluorescent

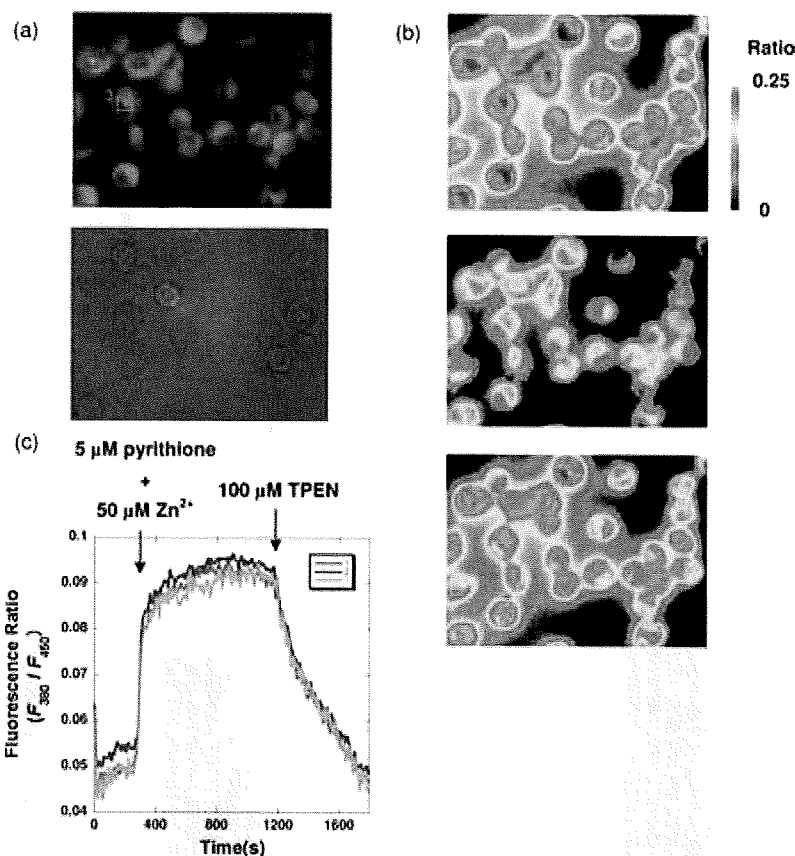


Figure 6. (a) Fluorescence microscopic image (λ_{ex} : 450 nm) (top), brightfield microscopic image (bottom), and (b) ratiometric fluorescence image (λ_{ex} : 380 and 450 nm) of RAW264 cells (top: 0 s, middle: 600 s, bottom: 1800 s) incubated with $10 \mu\text{M}$ **5** for 5 min at 37°C . The color coding scale means the fluorescence ratio values. (c) Time course of the ratiometric fluorescence values of the areas 1 (red), 2 (blue), and 3 (orange), which are indicated in (a).

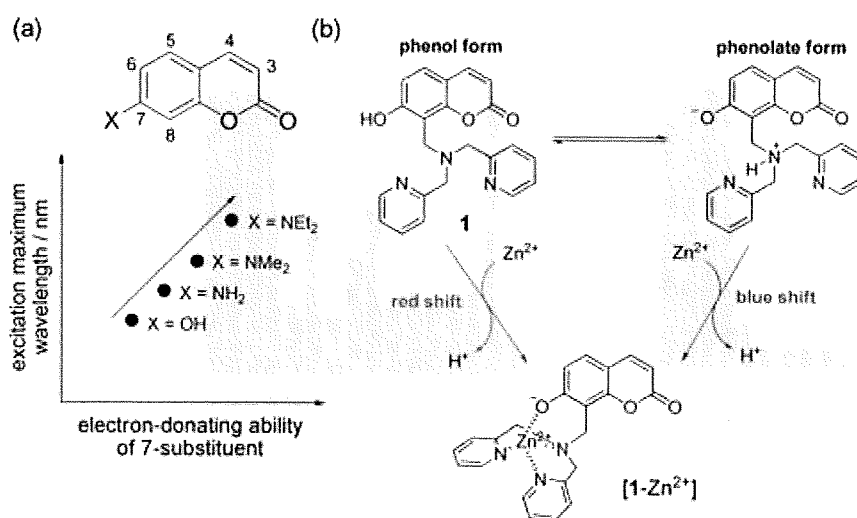


Figure 7. (a) Correlation between the electron-donating ability of 7-substituent and the excitation maximum wavelength of 7-substituted coumarins. (b) Two forms of probe **1** and the spectral change to the Zn^{2+} complex.

properties under physiological conditions. To achieve ratiometric Zn^{2+} -sensing, we focused our attention on the spectroscopic property of 7-substituted coumarins. As we had previously utilized the property for anion-sensing,¹⁸ the

absorbance and excitation spectra of the 7-substituted coumarin were affected by the functional substitution at the 7-position (Figure 7(a)).¹⁹ When the oxygen atom of 7-hydroxy group coordinates Zn^{2+} , the absorption and the excitation spectra are expected to shift toward either

(18) Mizukami, S.; Nagano, T.; Urano, Y.; Odani, A.; Kikuchi, K. *J. Am. Chem. Soc.* **2002**, *124*, 3920–3924.

(19) Wheelock, C. E. *J. Am. Chem. Soc.* **1959**, *81*, 1348–1352.

longer or shorter wavelengths, according to changes in electron-donating ability. The direction of the excitation spectral shift would be dependent on whether the 7-hydroxy group is protonated or deprotonated under the measurement condition. Since the electron-donating ability is expected to be increased in the order of $-\text{OH} < -\text{O}^- \cdots \text{Zn}^{2+} < -\text{O}^-$, we expected spectral changes as follows: When the phenol form is dominant, the complexation with Zn^{2+} would prompt red shifts in the spectra; when the phenolate form is dominant, Zn^{2+} complexation would prompt blue shifts (Figure 7(b)).

Zn²⁺-Sensing Properties of Probe 1. When Zn^{2+} was added to the solution of 5 μM **1**, the absorbance and the excitation spectra were shifted toward longer wavelengths (Supporting Information, Figure S1(a) and Figure 2(a), respectively). These results indicate that the 7-hydroxy group participated in the coordination with Zn^{2+} , and that the phenol form of **1** is dominant in 100 mM HEPES buffer (pH 7.4) (Figure 7(b)). This presumption was also confirmed by the pH profile measurement of the absorbance spectra (Figure 4(a)), where the peak top was around 330 nm at pH 7.4, as well as at a more acidic pH—although the peak top was around 370 nm at pH 9.5. The absorbance peak top of the 7-hydroxycoumarin was at 330 nm when the 7-hydroxy group was protonated, but shifted to 370 nm for the phenolate form.²⁰ According to the above mechanism, **1** made an excitation spectral shift toward a longer wavelength, with the addition of Zn^{2+} (Figure 2(a)); however, the spectral change was not ideal for ratiometric fluorescence imaging, because there was no clear isofluorescent point in the excitation spectra. On the other hand, an isosbestic point was observed in the absorbance spectra of **1** titrated with Zn^{2+} (Supporting Information, Figure S1(a)). This would be ascribed to the fluorescence quenching of **1**, because the fluorescence quantum yield (Φ) of **1** was lower than that of [**1**- Zn^{2+}] (Table 1). We considered the quenching to be the result of the photoinduced electron transfer (PET) from a DPA moiety, which would have been observed in known coumarin-based Zn^{2+} probes possessing a DPA ligand.^{16b,16d}

Introduction of Chlorine Atom at the 6-Position of Coumarin: Design and Properties of Probe 2. In the case of **1**, the phenol form was expected to be dominant in pH 7.4, as described above. Conversely if the phenolate form is dominant, it will induce a blue shift of the excitation spectra. We considered that the difference in the way of spectral shift might enable the ratiometric measurement. Thus, we designed compound **2**, in which a chlorine atom was introduced at the 6-position. The substitution of a chloro- or fluoro-group at the 6-position can decrease the $\text{p}K_a$ of 7-hydroxycoumarin via the inductive effect, and it was expected that the dominant form of **2** in pH 7.4 buffer was the deprotonated one.

The excitation spectral change of **2** (Figure 2(b)) showed that Zn^{2+} induced the blue shift of the excitation spectra. Also, the pH profile of the absorbance spectra of **2** indicated that the phenolate form of **2** was the dominant species at pH 7.4 because the absorbance maximum wavelength was 372 nm (Supporting Information, Figure S2(a)). Meanwhile, the difference in excitation maximum

wavelength between **2** and [**2**- Zn^{2+}] was only 6 nm; therefore, further improvement was desired in terms of practical ratiometric fluorescence measurement, although there was an isofluorescent point in the excitation spectral change.

Modification of the Ligand Structure: Designs and Properties of Probes 3 and 4. We attempted to change the Zn^{2+} ligand structure because the modification of the ligand structure might not only change the association constant among metal ions but also change the $\text{p}K_a$ of the hydroxy group near the ligand. We designed **3** and **4** with another ligand, *N,N*-dipicolylaminoethylamine. With regards to both **3** and **4**, the phenolate forms were dominant at pH 7.4 (Supporting Information, Figures S2(b) and S2(c)), and thus the addition of Zn^{2+} induced the blue shifts in the excitation spectra, as the case of **2** (Figures 2(c) and 2(d)).

The excitation maximum wavelengths of **3** and **4** were each 374 nm. When the probes bound Zn^{2+} ions, the spectral peak tops were shifted to 357 nm, and thus the spectral shifts were 17 nm each—much larger than had been the case with **1** or **2**. In the excitation spectra of **3** and **4**, in the presence of several concentrations of Zn^{2+} ion, there were isofluorescent points at 382 and 377 nm, respectively; therefore, they could serve as more practical ratiometric probes for Zn^{2+} ions. However, they are excitable only by UV light, which can cause damage to living cells and tissues. We therefore sought to improve further the probe structure for visible light excitation.

Design and Properties of Visible Light Excitation Probe 5. To achieve longer-wavelength excitation, further modification was required. Since deprotonated 3-benzothiazolyl-7-hydroxycoumarin is known to have strong absorption in the visible light region in polar solvent,²¹ we designed and synthesized **5** based on this structure. As expected, the excitation maximum of **5** was at 454 nm for the deprotonated form as well as for **3** and **4**, and at 432 nm for the Zn^{2+} complex (Figure 2(e)). The isofluorescent point of the excitation spectra was observed at 428 nm. Thus, this probe can be used for ratiometric fluorescence measurement of Zn^{2+} with visible light excitation, for example, at 400 and 450 nm. In addition to the ratiometric fluorescence property derived by exciting at two different wavelengths, probe **5** could also be applied to ratiometric measurement by monitoring at two emission wavelengths. Figure 3(e) shows the emission spectral change in the presence of Zn^{2+} ; the peak top shifted from 494 to 487 nm, with an isofluorescent point at 491 nm with Zn^{2+} addition. In passing, it should be noted that probe **4** also showed the same ratiometric emission properties.

Zn²⁺-binding Properties of Probes 1–5. To study the Zn^{2+} -binding properties of the probes, the binding stoichiometry to Zn^{2+} was investigated. Job's plots showed that all probes formed 1:1 complexes with Zn^{2+} (Supporting Information, Figure S3). The apparent dissociation constants with Zn^{2+} were as high as with the known Zn^{2+} probes. Concerning the correlation between ligand structure and the apparent binding constant to Zn^{2+} , the dipicolylaminoethylamino group showed a

(20) Fink, D. W.; Koehler, W. R. *Anal. Chem.* **1970**, *42*, 990–993.

(21) Azim, S. A.; Al-Hazmy, S. M.; Ebeid, E. M.; El-Daly, S. A. *Opt. Laser Technol.* **2005**, *37*, 245–249.

slightly higher binding constant than did the dipicolyl-amino group. The sensing selectivity to Zn^{2+} was sufficient for cellular application, although the ratiometric values of probes are largely changed by Cd^{2+} ions, because Cd^{2+} does not constitute an important metal ion in physiological studies. In the case of **5**, the ratio values change by a small amount in response to Fe^{3+} , Cu^{2+} , and Co^{2+} ; however, it is thought that these transition metal ions are generally bound to proteins and scarcely exist as free ions.

Cellular Application. To confirm whether **5** can detect intracellular Zn^{2+} under ratiometric fluorescence microscopy, we introduced the probe to RAW264 cells. Probe **5** could pass through the cell membrane without any modifications, as shown in Figure 6(a), probably because of the high lipophilicity involved. We then measured the change in ratiometric signal F_{380}/F_{450} by changing the intracellular Zn^{2+} concentration with pyrithione and TPEN. The results (Figure 6(b) and 6(c)) indicate that the probe enables the ratiometric detection of intracellular Zn^{2+} as quickly as the reported probes.^{7c,8b} Since there are few compounds that can achieve both visual light excitation and ratiometric imaging in cells, we expect this probe can be utilized for the ratiometric detection of Zn^{2+} concentration in living cells that are vulnerable to UV excitation.

Conclusion

We developed a series of coumarin-based fluorescent probes for detecting Zn^{2+} with high affinities. The design strategy was based on the fluorescent properties of 7-substituted coumarins. The ligands were introduced at the 8-position because of the ease of synthesis and the electrostatic effects in reducing the pK_a of 7-hydroxy groups. Additional substituents were incorporated into the 6- and/or 3-position to improve the properties. Among five developed probes, **2–5** showed the ratiometric fluorescent properties, and **5** could be excited at visible light wavelength. Using cell membrane permeable probe **5**, we confirmed the ratiometric fluorescence-sensing ability for free Zn^{2+} in living cells. We expect this probe will lead to the "next stage" of physiological Zn^{2+} studies, in both neurology and immunology, and so on.

Experimental Section

Materials and Instruments. The detailed synthesis procedures for **1–5** are described in Supporting Information. All reagents for synthesis and measurements were purchased from Tokyo Chemical Industries, Wako Pure Chemical, or Aldrich Chemical Co. All were of the highest grade available, and were used without further purification. Silica gel column chromatography was performed using BW-300, or Chromatorex NH (Fuji Silysia Chemical Ltd.). Cells were obtained from the Riken BRC Cell Bank, and reagents for culture were purchased from Gibco. NMR spectra were recorded on a JEOL JNM-EX270 instrument at 270 MHz for 1H NMR and at 64.5 MHz for ^{13}C NMR, or a JEOL JNM-AL400 instrument at 400 MHz for 1H and at 100.4 MHz for ^{13}C NMR, using tetramethylsilane as an internal standard. Mass spectra (CI, FAB) were measured on a JEOL JMS-700. ESI-TOF MS was taken on a Waters LCT-Premier XE. UV-visible spectra were measured using a Shimadzu UV-1650PC. Fluorescence spectra were measured using a Hitachi F4500 spectrometer. The slit width for both excitation and emission spectra was 5.0 nm. The photomultiplier voltage was 400 V. For ratiometric fluorescence images were recorded using

IX71 (Olympus) for the fluorescent microscope, Cool Snap HQ (Roper Scientific) for the cooled CCD camera, Polychrome V (TILL Photonics) for the xenon lamp with a monochromator, 470DCXRU (CHROMA) for the dichroic mirror, HQ515/50m-2p (CHROMA) for the emission filters, and MetaMorph (Universal Imaging Corporation) for the imaging software and data analysis.

Measurement of Photophysical Properties. All probes were prepared at 5 mM stock DMSO solution and diluted to the final concentration for each experiment. Zn^{2+} stock solution was prepared at 50 mM concentration by dissolving $ZnSO_4 \cdot 7H_2O$ in ultrapure water. Absorbance, excitation, and emission spectra were measured in 100 mM HEPES buffer (pH 7.4) at 25 °C. Quantum yields were calculated using quinine sulfate ($\Phi = 0.55$) in 0.5 M H_2SO_4 aq. or fluorescein ($\Phi = 0.92$) in 0.1 M NaOH aq. as the standard compounds, as described previously.²²

Preparation of Zn^{2+} - and pH-Buffered Solution. A series of 100 mM HEPES buffer (pH 7.4, $I = 0.1$ (NaNO₃)) were prepared containing 10 mM nitrilotriacetic acid (NTA) and 0–5.3 mM $ZnSO_4$. The apparent stability constant for NTA- Zn^{2+} complex β_1' is defined as follows: $\beta_1' = \beta_1/\alpha_M\alpha_L$, where β_1 is the stability constant for NTA- Zn^{2+} complex, $\alpha_M = 1 + 10^{(pH-pK_1)}$, $\alpha_L = 1 + 10^{(pKa_1-pH)} + 10^{(pKa_1+pKa_2-2pH)} + 10^{(pKa_1+pKa_2+pKa_3-3pH)}$. Regarding the pK_a of Zn^{2+} , $pK_1 = 9.0$,²³ and regarding the pK_a s of NTA, $pKa_1 = 9.74$, $pKa_2 = 2.48$, and $pKa_3 = 1.88$.²³ Protonation constants were corrected upward by 0.11 for 0.1 M of ionic strength.²⁴ The stability constant for NTA- Zn^{2+} complex: $\log \beta_1 = 10.4$.²³ Thus, $\alpha_M \approx 1$, $\alpha_L \approx 10^{2.34}$, $\beta_1' = \beta_1/\alpha_M\alpha_L = 10^{10.4}/10^{2.34} = 10^{8.06}$. Free Zn^{2+} concentration $[Zn^{2+}]_{free}$ was calculated as per the following equation.

$$[Zn^{2+}]_{free} = [Zn^{2+}]_{total}/(\beta_1'\alpha_M[NTA]_{free}) \\ = [Zn^{2+}]_{total}/\{\beta_1'\alpha_M([NTA]_{total} - [Zn^{2+}]_{total})\}$$

Determination of the Apparent Dissociation Constant (K_d) with Zn^{2+} . The fluorescence intensity F of the probes were plotted against $[Zn^{2+}]_{free}$, the concentration of free Zn^{2+} . The apparent dissociation constants K_d s with Zn^{2+} were determined by fitting the data to the following equation:

$$F = F_0 + (F_{max} - F_0)[Zn^{2+}]_{free}/(K_d + [Zn^{2+}]_{free})$$

where F is the observed fluorescence intensity, F_0 is the fluorescence intensity without Zn^{2+} , F_{max} is the maximum fluorescence intensity, and $[Zn^{2+}]_{free}$ is the concentration of free Zn^{2+} .

Effect of pH on Fluorescence Properties. We measured the fluorescence intensity of the probes in 10 mM phosphate buffer aqueous solution showing several pH values (pH 4.4–12.5). The fluorescence intensities were plotted against solution pH.

Metal Ion Selectivity. The fluorescence intensity and ratio values were measured in 100 mM HEPES buffer (pH 7.4). The probe concentration was 5 μ M for **1–4** or 1 μ M for **5**. The stock solutions of Na^+ , K^+ , Ca^{2+} , and Mg^{2+} were prepared at 500 mM and diluted to final concentrations (5 mM or 1 mM). The stock solution of Mn^{2+} , Fe^{3+} , Co^{2+} , Ni^{2+} , Cu^{2+} , Zn^{2+} , and Cd^{2+} were prepared at 5 mM and diluted to final concentrations (5 μ M or 1 μ M).

Cell Cultures and Live Cell Imaging. RAW264 cells were cultured in MEM containing 10% fetal bovine serum, 1% penicillin, 1% streptomycin, and 0.1 mM MEM non-essential amino acid solution at 37 °C in a 5% CO₂ incubator. The cells

(22) Dawson, R. W.; Windsor, W. M. *J. Phys. Chem.* 1968, 72, 3251–3260.

(23) Perin, D. D.; Dempsey, B. *Buffers for pH and Metal Ion Control*; John Wiley & Sons, Chapman and Hall: New York and London, 1974.

(24) Martell, A. E.; Smith, R. M. *NIST Critical Stability Constants of Metal Complexes, NIST Standard Reference Database*; Plenum Press: New York and London, 1974; Vol. 1.

were transferred to a glass-bottomed dish and incubated for 1 day before dye-loading. The cells were washed with PBS twice and incubated with PBS containing 10 μM probes for 5 min at 37 °C. The cells were then washed with PBS twice, and measurements were carried out with fluorescence microscope. A total of 5 μM pyrithione and 50 μM Zn^{2+} were treated to increase intracellular Zn^{2+} concentration, $[\text{Zn}^{2+}]_i$, and 100 μM TPEN was treated to decrease $[\text{Zn}^{2+}]_i$ by chelating.

Acknowledgment. This work was supported in part by the Ministry of Education, Culture, Sports, Science and Technology (MEXT) of Japan (Grants 18310144, 18032045, 18033034, 18011005, 19036012, 19021028, 19651093 to K.K. and 19710185 to S.M.). This work was also supported by the Special Coordination Funds for the Council of Science and Technology Policy

Coordination Program of Science and Technology Projects, MEXT and JST, to K.K. K.K. was also supported by the Mitsubishi Foundation, by the Novartis Foundation for the Promotion of Science, by Shimadzu Science Foundation, by Kato Memorial Bioscience Foundation, by Astellas Foundation for Research on Metabolic Disorders, by the Uehara Memorial Foundation, by Terumo Life Science Foundation, by Nagase Science and Technology Foundation, and by the Asahi Glass Foundation. S.M. was supported by the Cosmetology Research Foundation.

Supporting Information Available: Detailed synthetic procedures of compounds, and supplementary figures. This material is available free of charge via the Internet at <http://pubs.acs.org>.